Angiopoietin-1 is required for Schlemm's canal development in mice and humans

Benjamin R. Thomson,[1,2] Tomokazu Souma,[1,2] Stuart W. Tompson,[3] Tuncer Onay,[1,2] Krishnakumar Kizhatil,[4] Owen M. Siggs,[5] Liang Feng,[6] Kristina N. Whisenhunt,[3] Tammy L. Yanovitch,[7] Luba Kalaydjieva,[8] Dimitar N. Azmanov,[8,9] Simone Finzi,[10] Christine E. Tanna,[1,2] Alex W. Hewitt,[11,12,13] David A. Mackey,[12,13] Yasmin S. Bradfield,[3] Emmanuelle Souzeau,[5] Shari Javadiyan,[5] Janey L. Wiggs,[14] Francesca Pasutto,[15] Xiaorong Liu,[6] Simon W.M. John,[4] Jamie E. Craig,[5] Jing Jin,[1,2] Terri L. Young,[3] and Susan E. Quaggin[1,2]

[1]Feinberg Cardiovascular Research Institute and [2]Division of Nephrology/Hypertension, Northwestern University Feinberg School of Medicine, Chicago, Illinois, USA. [3]Department of Ophthalmology and Visual Sciences, University of Wisconsin–Madison, Madison, Wisconsin, USA. [4]Howard Hughes Medical Institute and The Jackson Laboratory, Bar Harbor, Maine, USA. [5]Department of Ophthalmology, Flinders University, Adelaide, South Australia, Australia. [6]Department of Ophthalmology, Northwestern University Feinberg School of Medicine, Chicago, Illinois, USA. [7]Department of Ophthalmology, Dean McGee Eye Institute, University of Oklahoma, Oklahoma City, Oklahoma, USA. [8]Harry Perkins Institute of Medical Research and Centre for Medical Research, University of Western Australia, Perth, Western Australia, Australia. [9]Department of Diagnostic Genomics, PathWest, QEII Medical Centre, Perth, Western Australia, Australia. [10]Department of Ophthalmology, Hospital das Clínicas of University of São Paulo, São Paulo, Brazil. [11]Centre for Eye Research Australia, University of Melbourne, Royal Victorian Eye and Ear Hospital, Melbourne, Victoria, Australia. [12]Centre for Ophthalmology and Visual Science, University of Western Australia, Lions Eye Institute, Perth, Western Australia, Australia. [13]Menzies Institute for Medical Research, University of Tasmania, Hobart, Tasmania, Australia. [14]Department of Ophthalmology, Massachusetts Eye and Ear Infirmary, Harvard Medical School, Boston, Massachusetts, USA. [15]Institute of Human Genetics, Friedrich-Alexander-Universität Erlangen-Nürnberg, Erlangen, Germany.

Primary congenital glaucoma (PCG) is a leading cause of blindness in children worldwide and is caused by developmental defects in 2 aqueous humor outflow structures, Schlemm's canal (SC) and the trabecular meshwork. We previously identified loss-of-function mutations in the angiopoietin (ANGPT) receptor *TEK* in families with PCG and showed that ANGPT/TEK signaling is essential for SC development. Here, we describe roles for the major ANGPT ligands in the development of the aqueous outflow pathway. We determined that ANGPT1 is essential for SC development, and that *Angpt1*-knockout mice form a severely hypomorphic canal with elevated intraocular pressure. By contrast, ANGPT2 was dispensable, although mice deficient in both *Angpt1* and *Angpt2* completely lacked SC, indicating that ANGPT2 compensates for the loss of ANGPT1. In addition, we identified 3 human subjects with rare *ANGPT1* variants within an international cohort of 284 PCG patients. Loss of function in 2 of the 3 patient alleles was observed by functional analysis of ANGPT1 variants in a combined in silico, in vitro, and in vivo approach, supporting a causative role for ANGPT1 in disease. By linking ANGPT1 with PCG, these results highlight the importance of ANGPT/TEK signaling in glaucoma pathogenesis and identify a candidate target for therapeutic development.

Introduction

Afflicting more than 60 million individuals worldwide and leaving 8 million blind, glaucoma is a devastating disease with no cure (1). Current therapy slows disease progression but cannot repair the damage to retinal ganglion cells — underscoring the urgent unmet need for new drug targets and treatments. Elevated intraocular pressure (IOP) is an important risk factor for glaucoma, and patients with high-pressure glaucoma exhibit defects in aqueous humor drainage from the anterior chamber (2, 3). Aqueous humor is secreted by the ciliary body before entering the anterior chamber, where it is drained through outflow structures in the iridocorneal angle. Decreased flow through these pathways creates an imbalance in fluid homeostasis, leading to ocular hypertension and glaucoma. In humans, the majority of aqueous humor outflow is carried out through the conventional route, composed of the trabecular meshwork (TM) and Schlemm's canal (SC), a large, hybrid vessel with lymphatic and venous features located within the iridocorneal angle (4–6). Despite the central role of SC in IOP maintenance and disease, no pharmacological tools targeting the canal are currently available in the clinic. Recently, however, the importance of endothelial growth factor signaling has been appreciated, and critical roles for both the VEGF/VEGFR and the ANGPT/TEK pathway have been described (5–8), identifying an array of potential targets for future therapeutic development.

The angiopoietin (ANGPT)/TEK (tunica interna endothelial cell kinase, also known as TIE2) signaling pathway is composed of 3 ligands (ANGPT1, ANGPT2, and ANGPT4) and 2 receptors (TEK and TIE) (9, 10). Loss-of-function mutations in the endothelial receptor tyrosine kinase TEK, which is highly expressed

Authorship note: B.R. Thomson and T. Souma contributed equally to this work. T.L. Young and S.E. Quaggin contributed equally to this work.
Conflict of interest: S.E. Quaggin holds patents (US patent US9719135B2) related to therapeutic targeting of the ANGPT/TEK pathway in ocular hypertension and glaucoma and receives research support from, owns stock in, and is a director of Mannin Research.
Submitted: June 12, 2017; **Accepted:** September 26, 2017.
Reference information: *J Clin Invest*. 2017;127(12):4421–4436.
https://doi.org/10.1172/JCI95545.

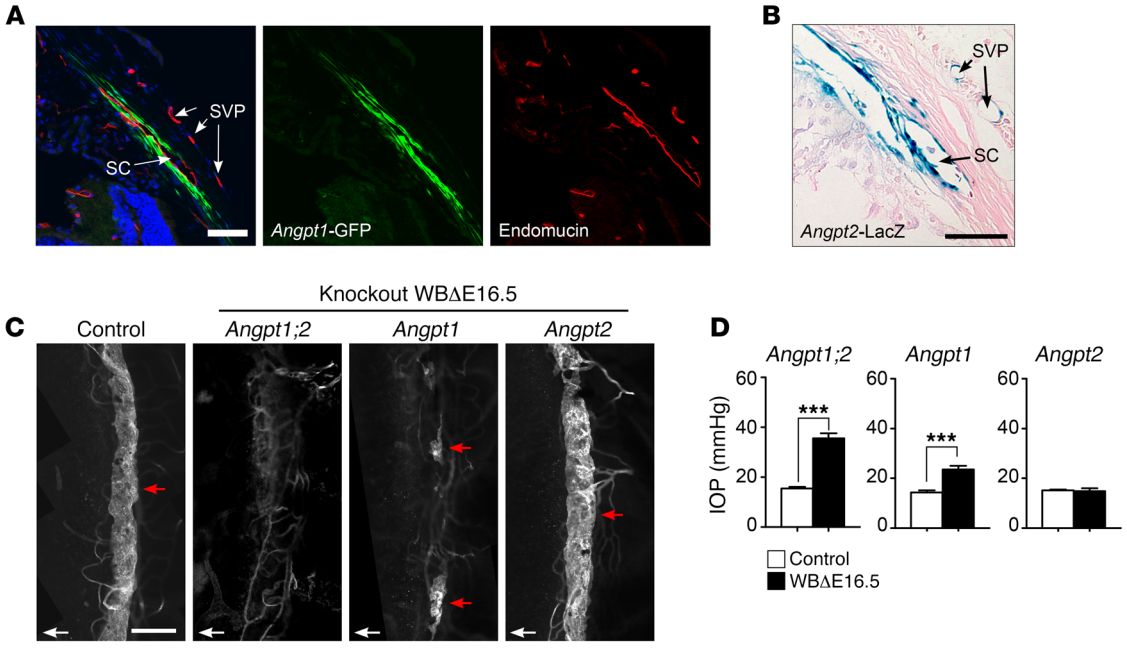

Figure 1. ANGPT1 is the primary TEK ligand in SC development. (**A**) Localization of *Angpt1* expression in the limbal region. Cryosections from adult *Angpt1*^{GFP} knockin mice show strong GFP expression in the TM and cells adjacent to the SC outer wall. Endomucin staining outlines the SC endothelium and capillaries of the superficial vascular plexus (SVP). (**B**) *Angpt2* expression in the anterior chamber. Paraffin sections from adult X-gal–stained *Angpt2*^{LacZ} knock-in mice show X-gal staining in the SC and corneal endothelium, as well as capillaries of the SVP. (**C**) In comparison with control littermates, eyes from mice with defective angiopoietin signaling failed to develop a normal SC. As previously described, *Angpt1 Angpt2* double-knockout (*Angpt1;2*) mice completely lacked SC. Interestingly, however, while *Angpt1*$^{WBΔE16.5}$ mice exhibited a severely hypoplastic canal with only focal development, *Angpt2*$^{WBΔE16.5}$ mice had no apparent defect. (**D**) IOP measurements showed similar results (*Angpt1 Angpt2* n = 12, control n = 42; *Angpt1* n = 7, control n = 14; *Angpt2* n = 3, control n = 4). This highlights the role of ANGPT1 as the major TEK ligand in canal development, though it suggests the possibility of limited compensation. Red arrows in **C** highlight SC. White arrows indicate the direction of the cornea. Note that faint staining in *Angpt1;2* and *Angpt1* knockout panels is out of focus light from the ciliary body and limbal vascular plexus. Scale bars: 50 μm (**A** and **B**) and 250 μm (**C**). ***$P \leq 0.001$ as determined by Welch's t test.

in the SC endothelium (5), have been identified in patients with primary congenital glaucoma (PCG), an especially devastating form of the disease characterized by infant/early-childhood onset, buphthalmos, and optic neuropathy (8). In mice, loss of TEK signaling through either deletion of both primary ANGPT ligands or deletion of the TEK receptor results in failure of SC development and rapidly progressing ocular hypertension (7, 8). However, while the importance of ANGPT/TEK signaling in canal development and associated aqueous humor drainage is clear, the individual roles for each of the major ANGPT ligands are not understood.

Outside of the iridocorneal angle, ANGPT1 is expressed by pericytes and other vascular supporting cells, but not in the endothelium (11). It has been described as the primary TEK agonist, activating the receptor to drive its proangiogenic and vessel stabilizing activity (9, 12, 13). The other major ligand, ANGPT2, is a context-dependent agonist/antagonist of TEK signaling secreted by the endothelium as well as vascular supporting cells in specific vascular beds such as the renal mesangium and smooth muscle cells (9, 13–16).

Here, we describe the individual roles of ANGPT1 and ANGPT2 in SC development and identify ANGPT1 as the primary TEK ligand in canal formation. Furthermore, we have identified and characterized human *ANGPT1* loss-of-function mutations in a PCG cohort of 284 families that did not harbor mutations in the known PCG-causing genes *CYP1B1* or *TEK*.

Results

Angpt1 and Angpt2 are expressed in the iridocorneal angle. To better understand the role of each ANGPT ligand in SC development and function, we analyzed their expression pattern in the limbus using *Angpt1*^{GFP} and *Angpt2*^{LacZ} reporter mice. *Angpt1* is expressed in the TM and in cells adjacent to the SC outer wall, although no expression is seen in the endomucin-positive SC endothelium (Figure 1A). Conversely, *Angpt2* is expressed by the SC endothelium, as well as by endothelial cells of limbal capillaries and the corneal endothelium (Figure 1B).

ANGPT1 is the primary TEK ligand in the iridocorneal angle. As both *Angpt1* and *Angpt2* are highly expressed in the iridocorneal angle, we used a knockout mouse approach to discover a specific role(s) for each ligand in canal formation. Mice lacking *Angpt1*, *Angpt2*, or both *Angpt1* and *Angpt2* after embryonic day 16.5 (WBΔE16.5) were generated using a doxycycline-based conditional gene targeting strategy as previously described (7). Lacking suitable antibodies for Western blot, knockout was confirmed using real-time PCR (Supplemental Figure 1; supplemental material available online with this article; https://doi.org/10.1172/JCI95545DS1). While control mice exhibit a continuous CD31-positive SC, confocal microscopy revealed complete absence of SC in *Angpt1;Angpt2* double-knockout mice (*Angpt1;Angpt2*$^{WBΔE16.5}$) (Figure 1C). Similarly, *Angpt1*$^{WBΔE16.5}$ mice exhibited a severely hypoplastic SC phenotype characterized by gaps and discontinuous, isolated canal segments. While this phenotype was less severe than

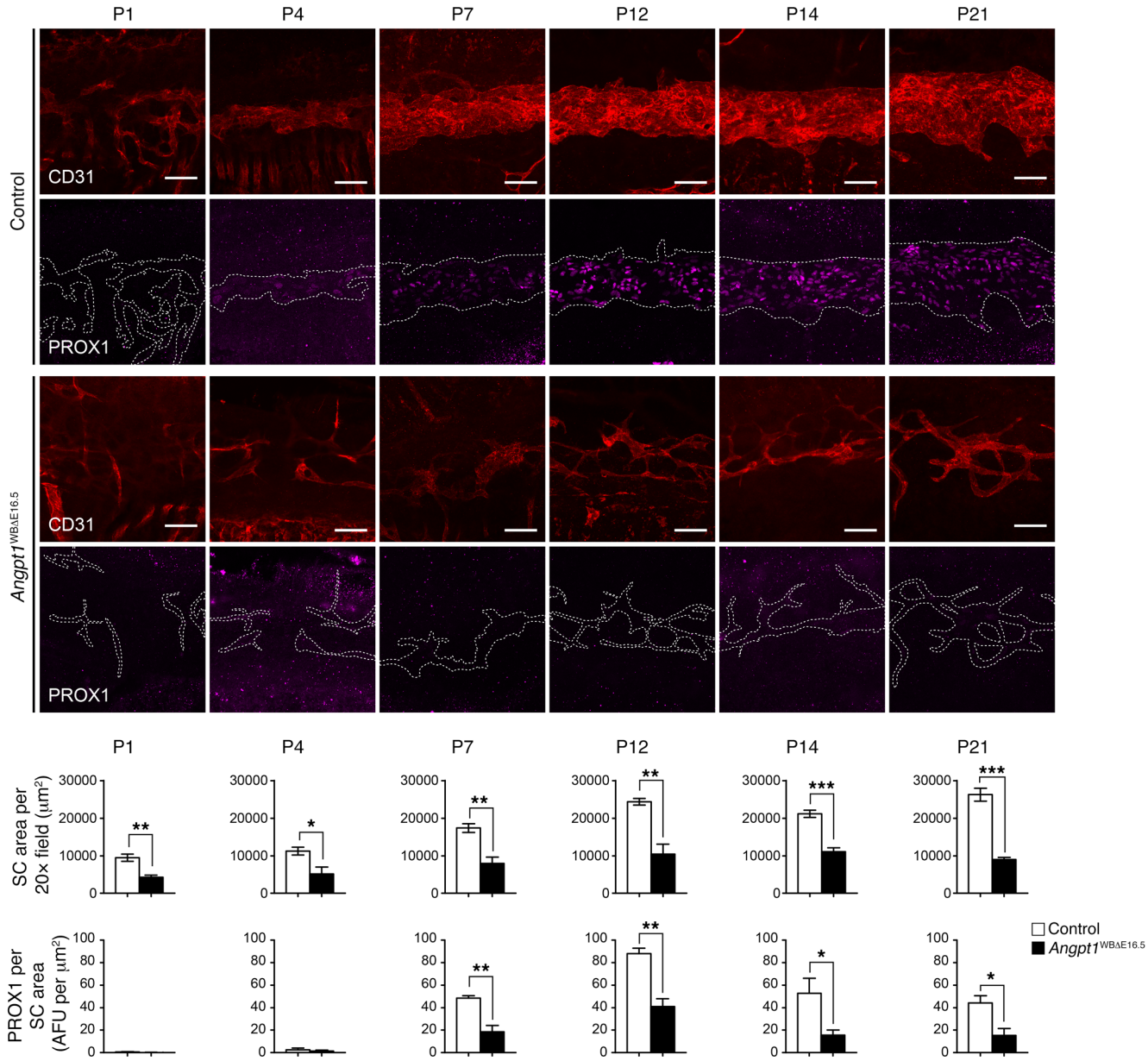

Figure 2. ANGPT1 is essential for SC formation. SC development and maturation in *Angpt1*-knockout mice. Compared with littermate controls, SC development was disrupted in *Angpt1*$^{WB\Delta E16.5}$ mice. Fewer CD31-positive sprouts emerge from the limbal capillaries, and these sprouts failed to consolidate and proliferate into a cohesive SC. In addition, PROX1 expression was dramatically reduced in the disorganized SC plexus of mutant mice, indicating that these cells failed to differentiate into the mature SC cell fate. Dashed lines in PROX1 panels highlight the CD31-positive sprout and SC area from matching CD31 staining. Littermate controls were used for all time points; eyes from 3 knockout and 3 control mice (P1, P12), 4 knockouts and 4 controls (P4), 6 knockouts and 5 controls (P7), 4 knockouts and 5 controls (P14), and 4 knockouts and 3 controls (P21) were analyzed. Three fields were captured per eye, and the results were averaged. AFU, background subtracted arbitrary fluorescence units. Scale bars: 50 μm; ×20 fields comprise an area of 65,536 μm^2. *$P \le 0.05$, **$P \le 0.01$, ***$P \le 0.001$ as determined by Student's *t* test.

that observed in *Angpt1;Angpt2* double knockouts, a clear requirement for ANGPT1 was observed. In contrast, SC had no apparent morphological defects in *Angpt2*-knockout mice. To determine the consequence of these SC defects for aqueous humor homeostasis, IOP was measured in *Angpt1*, *Angpt2*, and *Angpt1;Angpt2*-knockout mice at 8 weeks of age (Figure 1D). *Angpt1;Angpt2*$^{WB\Delta E16.5}$ mice presented with dramatic IOP elevation (*Angpt1;Angpt2*$^{WB\Delta E16.5}$, 35.58 ± 2.01 mmHg; controls, 15.45 ± 0.72; $P < 0.0001$). By contrast, *Angpt1* knockouts exhibited only moderately elevated pressure (*Angpt1*$^{WB\Delta E16.5}$, 23.53 ± 1.50 mmHg; controls, 14.29 ± 0.92 mmHg; $P = 0.0004$). Notably, despite the difference between *Angpt1;Angpt2* and *Angpt1* knockouts, *Angpt2*-knockout mice exhibited normal IOP (*Angpt2*$^{WB\Delta E16.5}$, 15.13 ± 0.41; control, 14.94 ± 1.01; $P = 0.882$), supporting the dispensable role of ANGPT2 in SC development and function.

ANGPT1 is required for development of SC and the TM. Our findings showed that ANGPT1 is a critical regulator of SC morphology and function, but did not distinguish between developmental and

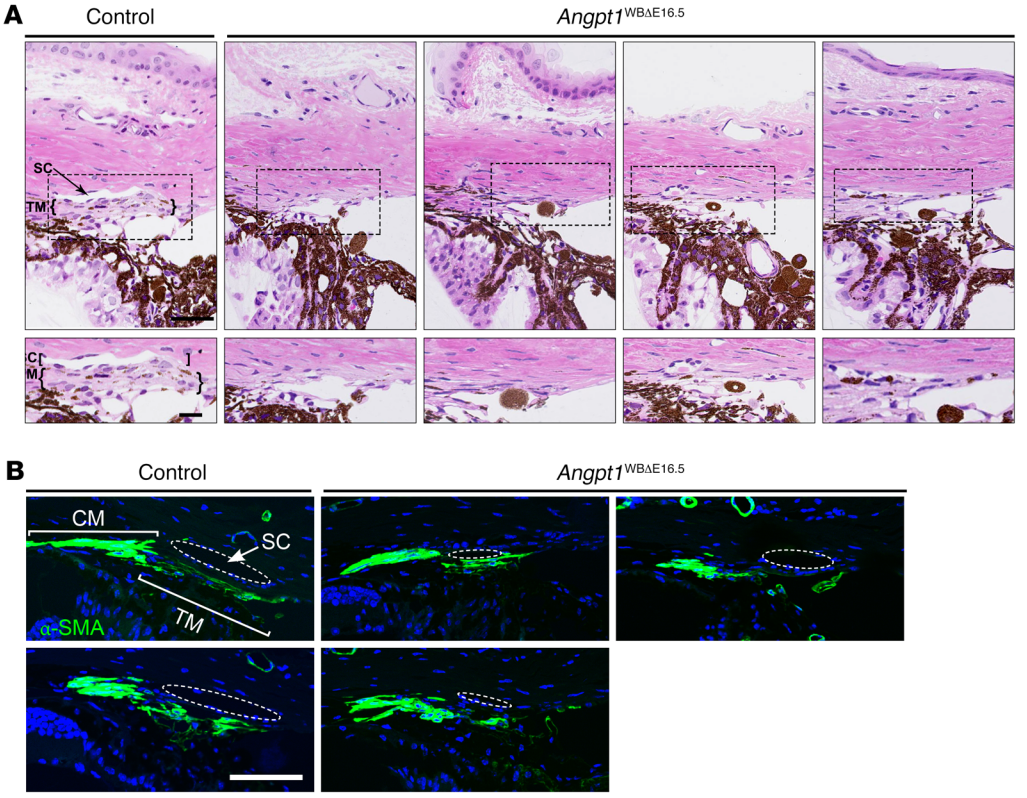

Figure 3. SC and the TM are defective in *Angpt1*$^{WB\Delta E16.5}$ mice. (**A**) Iridocorneal angle region from control and *Angpt1*$^{WB\Delta E16.5}$ mouse eyes obtained after imaging of plastic sections of eyes stained with H&E. Top panels show the location of SC and the TM within the iridocorneal angle. Magnified images of the region within the dotted box in the top panels are shown below for each panel. The control showed a well-developed SC and TM in contrast to mutants, in which the TM was hypoplastic and the SC was either absent or severely reduced in size. Control $n = 4$, *Angpt1*$^{WB\Delta E16.5}$ $n = 8$. Scale bars: top panels, 50 μm, and bottom panels, 10 μm. (**B**) α-Smooth muscle actin–stained (α-SMA–stained) sections of the iridocorneal angle region from control and *Angpt1*$^{WB\Delta E16.5}$ eyes, showing the ciliary muscle (CM) and TM. SC is indicated by a dashed oval. As in **A**, eyes lacking *Angpt1* showed dramatic reduction in the size of SC and associated TM. Scale bar: 250 μm.

degenerative phenotypes. To determine the role of ANGPT1 in canal development, eyes were collected at intervals from birth to P21 and canal morphology was observed by confocal microscopy. SC forms in the postnatal period from sprouts that branch off the limbal vascular plexus (LVP); at P1, the LVPs of *Angpt1*$^{WB\Delta E16.5}$ eyes were found to have significantly reduced pre-SC endothelial sprouting in comparison with control littermates, in both total area (Figure 2) and sprout number (Supplemental Figure 2). Interestingly, the LVP area appeared normal in *Angpt1*$^{WB\Delta E16.5}$ mice, which suggested that these sprouting defects were unique to SC development and were not due to a failure in LVP capillary or global endothelial sprouting (Supplemental Figure 3). By P4, the difference between mutant and control SC became more pronounced. At this time point, consolidation of sprouting endothelial cells into a canal-like structure was apparent in control mice, whereas in *Angpt1*$^{WB\Delta E16.5}$ littermates the endothelial cells remained disorganized with no apparent canal structure (Figure 2). This trend continued throughout development as, compared with controls, knockout mice began with a smaller pool of sprouting SC progenitor cells and never exhibited the increased proliferation required to overcome this handicap and form a complete canal (Supplemental Figure 4). In control mice, between P4 and P7, SC endothelial cells began to differentiate into a clear SC cell fate, expressing the lymphatic marker PROX1 (Figure 2). However, this differentiation did not take place in the vestigial canal structure observed in knockout mice, and PROX1 expression remained low. By adulthood, only isolated segments of canal endothelium were observed in knockout mice. Importantly, each of these remaining segments was connected to the limbal blood vascular plexus by at least 1 drainage channel, suggesting that the residual SC fragments may retain some function (Supplemental Figure 5).

To examine the effect of *Angpt1* deletion on TM development, plastic semithin sections were prepared from the iridocorneal region and stained with H&E. While control littermates showed a well-developed SC and TM, *Angpt1*$^{WB\Delta E16.5}$ mice exhibited a small or absent SC associated with a severely hypoplastic TM (Figure 3A). Immunofluorescent staining using an antibody against α-smooth muscle actin, which specifically labels the ciliary muscle and TM, highlighted this TM defect (Figure 3B).

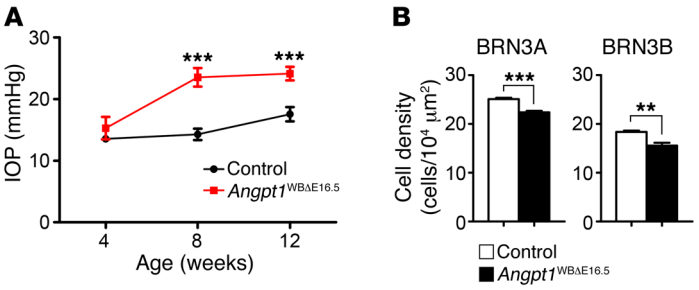

Figure 4. *Angpt1*-knockout mice exhibit clinical signs of glaucoma. (**A**) Intraocular pressure (IOP) of *Angpt1*-knockout mice. Compared with control littermates, *Angpt1*$^{WB\Delta E16.5}$ mice rapidly developed elevated IOP. *Angpt1*$^{WB\Delta E16.5}$ $n = 7$, control $n = 13$. (**B**) Measurement of retinal ganglion cell number. When dissected at 19 weeks, mice lacking *Angpt1* exhibited significant reductions in retinal ganglion cells compared with littermate controls. *Angpt1*$^{WB\Delta E16.5}$ $n = 5$, control $n = 4$. $^{**}P \le 0.01$, $^{***}P \le 0.001$ as determined by 2-way ANOVA followed by Bonferroni's correction (**A**) or Student's *t* test (**B**).

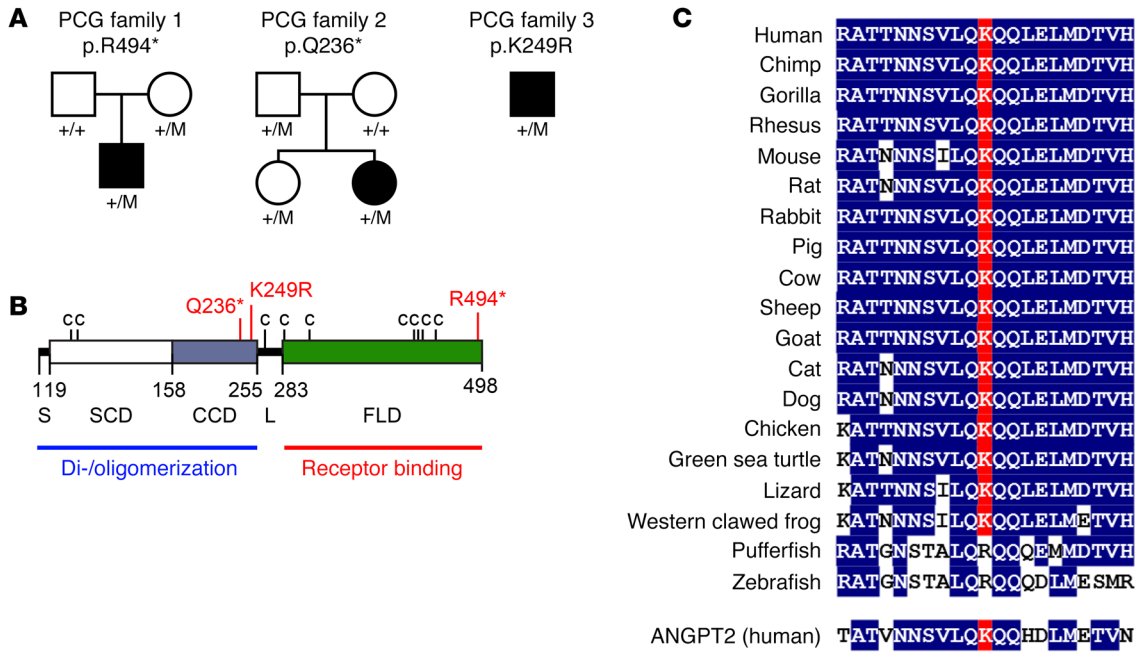

Figure 5. Pedigrees and *ANGPT1* variants identified in 3 families. (**A**) Pedigrees of 3 families with ANGPT1 mutations. Specific mutations in *ANGPT1* are listed below the different pedigrees, with carrier family members annotated as +/M. Affected individuals are indicated by solid black symbols. Note: White symbols do not exclude an undiagnosed late-onset disease. Parental genotypes/phenotypes are unknown for family 3. (**B**) Schematic representation of ANGPT1 protein domains and identified mutations in this study. S, signal peptide; SCD, superclustering domain; CCD, coiled-coil domain; L, linker domain; FLD, fibrinogen-like domain. (**C**) Sequence alignment of ANGPT1 K249 showing strong evolutionary conservation.

Angpt1-knockout mice develop a glaucoma-like phenotype. To determine the link between SC development and anterior chamber drainage, IOP was measured over time in a cohort of 7 *Angpt1*$^{WB\Delta E16.5}$ and 13 control mice (Figure 4A). While the initial measurement at 4 weeks showed no difference in IOP, subsequent measurements at 8 and 12 weeks revealed a marked IOP elevation in *Angpt1*$^{WB\Delta E16.5}$ mice (8 weeks: *Angpt1*$^{WB\Delta E16.5}$, 23.53 ± 1.50; control, 14.29 ± 0.92; $P < 0.001$; 12 weeks: *Angpt1*$^{WB\Delta E16.5}$, 24.143 ± 1.06; control, 17.55 ± 1.16; $P < 0.001$). As elevated IOP is strongly correlated with glaucoma pathogenesis, we next performed a series of studies to look for signs of glaucoma in a second cohort of *Angpt1*$^{WB\Delta E16.5}$ mice. Retinal ganglion cells (RGCs) were examined by immunohistochemistry, using antibodies against BRN3A and BRN3B, markers specific for RGCs. At 19 weeks, knockout mice had reductions in BRN3A-labeled RGC counts compared with their WT control littermates (Figure 4B; *Angpt1*$^{WB\Delta E16.5}$, 22.38 ± 0.30; control, 25.09 ± 0.28; $P = 0.0003$). Similar reductions were found in BRN3B cell density (*Angpt1*$^{WB\Delta E16.5}$, 15.57 ± 0.58; control, 18.35 ± 0.29; $P = 0.0053$). Taken together these results are consistent with glaucomatous neurodegeneration, although further studies will be required to fully characterize the glaucoma phenotype in *Angpt1*$^{WB\Delta E16.5}$ mice.

Loss-of-function mutations in ANGPT1 are associated with human PCG. SC defects observed in *Angpt1*$^{WB\Delta E16.5}$ mice, including narrowing, gaps, and rarefication of the TM, resemble a more severe form of the phenotypes previously described in mice heterozygous for the gene encoding the ANGPT1 receptor TEK. This similarity between mouse phenotypes suggested that, like mutations in *TEK*, loss-of-function mutations in *ANGPT1* may contribute to glaucoma pathogenesis in humans. To investigate this possibility, the *ANGPT1* gene was sequenced in a cohort of 284 PCG families with no mutations in the most commonly mutated PCG genes, including *CYP1B1* and *TEK*. Of this cohort, exome sequence data were available for 135 families, while direct Sanger sequencing of the *ANGPT1* gene was performed on the remaining 149. In addition to *CYP1B1* and *TEK*, exome-sequenced cases were also screened for rare PCG-associated mutations in *LTBP2*, *FOXC1*, and *MYOC* as well as novel, PCG-associated mutations in *ANGPT2* and *ANGPT4*. Variant data were filtered to remove synonymous changes, intronic variants more than 10 nucleotides from the intron-exon splice site junctions, variants present in the Exome Aggregation Consortium (ExAC) public database (exac.broadinstitute.org) at an allele frequency greater than 0.0001, and variants identified in an in-house database of 120 control exomes. The remaining variants identified through exome sequencing were validated by Sanger sequencing.

Heterozygosity for 2 novel nonsense variants (p.Q236*, p.R494*) and 1 rare missense variant (p.K249R) was identified in *ANGPT1* in 3 PCG families (Figure 5A and Table 1), while no novel PCG-associated variants were identified in *ANGPT2* or *ANGPT4*. In humans, the *ANGPT1* gene encodes a principal protein product of 498 amino acids in 9 exons. Each of the patient variants identified was predicted to affect this protein product in markedly different ways (Figure 5B). p.Q236* introduced a stop codon prematurely within exon 4 of the mRNA transcript. Truncated transcripts produced by this variant allele are expected to be recognized by the nonsense-mediated decay (NMD) pathway and eliminated. Any transcripts that are translated into protein would

Table 1. *ANGPT1* variants identified in PCG families

ID	Coding DNA modification	Protein alteration	Chromosome position	Exon	Age at onset	Carrier age	Eyes affected	Sex	Ethnicity	Allele count	ExAC Total alleles	ExAC Ethnically matched alleles
1	c.1480C>T	p.R494*	108264100	9	2 yr	41 yr	N/A	M	Eur (Am)	Novel[A]	121,306	66,690
2	c.706C>T	p.Q236*	108334226	4	Birth	N/A	2	F	Eur (Au)	Novel[B]	121,360	66,718
3	c.746A>G	p.K249R	108334186	4	Birth	N/A	2	M	Afr (Au)	1 (SA)	121,376	10,406

Ethnicities: Eur, European; Afr, African; Am, American; Au, Australian; SA, South Asian. ExAC, Exome Aggregation Consortium database; N/A, data not available. Carrier age, age of unaffected mutation carrier at time of last eye exam. Chromosome position is listed in accordance with the human GRCh37/hg19 reference assembly. Coding DNA mutation is in relation to *ANGPT1* mRNA reference sequence NM_001146.3. Protein change is in relation to ANGPT1 protein reference sequence NP_001137.2. [A]c.1480C>T is a known variant (rs144684252) in the National Heart, Lung, and Blood Institute Exome Sequencing Project (ESP) data set, identified in 1 of 8,600 European alleles. [B]c.706C>T was identified in a single in-house Australian control sample.

result in a truncated product containing the N-terminal oligomerization domain, but lacking the full C-terminal receptor binding domain that is essential for interaction with the TEK receptor. Conversely, the p.R494* variant introduces a stop codon just 5 residues prior to the normal termination codon in exon 9, and will likely escape NMD as premature truncations located in the final exon do not induce this mRNA cleanup system (17). The resulting protein product would contain the complete oligomerization domain, but lack the terminal 5 amino acids of the receptor binding domain. While ANGPT1^{R494*} may be capable of interacting with the TEK receptor, these 5 amino acids are highly conserved throughout vertebrate evolution (Supplemental Figure 6), and their deletion was predicted by FoldX to strongly destabilize the protein (FoldX score 5.36).

Unlike the 2 nonsense variants, the p.K249R missense variant was predicted to be tolerated by SIFT (sift.jcvi.org) and FATHMM (fathmm.biocompute.org.uk) with no expected effect on protein function. However, K249 is evolutionarily well conserved (Figure 5C), and this mutation has been observed only once (in a South Asian individual) out of more than 121,000 alleles in the ExAC database. Owing to the location of this modified amino acid, we predicted that ANGPT1^{K249R} might be unable to properly oligomerize, which is important for its ability to activate TEK (18–20).

To determine whether these variant ANGPT1 proteins have a reduced ability to activate TEK signaling, we generated heterologous expression vectors for WT and variant ANGPT1 proteins in cell culture models (Supplemental Figure 7) and performed in vitro assays to examine expression, intracellular trafficking, and signaling function. In vivo, WT ANGPT1 is a soluble growth factor secreted by pericytes, podocytes, and other vascular support cells. When heterologously expressed in HEK293 cells, WT ANGPT1 was produced and readily secreted into the growth medium, where it was detected using a C-terminal FLAG tag as previously reported (ANGPT1-FLAG; Figure 6A and ref. 18).

By SDS-PAGE, ANGPT1-FLAG monomers were found to run at approximately 75 kDa (Figure 6A). However, under nonreducing conditions, WT ANGPT1 protein was predominantly grouped in high-order multimers of greater than 250 kDa, consistent with earlier reports (18, 21). A similar multimerization pattern was observed in ANGPT1^{K249R}-FLAG variant protein, which was robustly expressed and secreted into the cell medium. Unlike the missense K249R variant, ANGPT1^{Q236*}-FLAG contains a premature stop codon upstream of the expression vector FLAG tag (Supplemental Figure 7B). As expected, this stop codon prevented production of full-length FLAG-labeled mutant protein, and none was observed in the media (Figure 6A), although unlabeled, truncated protein product may have been produced. Unlike the ANGPT1^{Q236*}-FLAG construct, the tagged ANGPT1^{R494*} construct was designed by insertion of the FLAG tag directly following I493 to create ANGPT1^{R494_F498del}-FLAG. Interestingly, no secreted ANGPT1^{R494_F498del}-FLAG protein could be detected following transfection in HEK293 cells. This was surprising given the location of the mutation in the C-terminal fibrinogen domain, and we had not anticipated a defect in secretion. We hypothesized that this mutant protein may be trapped within the cell or subject to premature degradation.

To test the ability of each ANGPT1 variant protein to activate TEK and initiate a downstream signaling cascade, conditioned medium from transfected HEK293 cells was used to stimulate primary HUVECs, which express TEK (Figure 6B). Consistent with the expression and oligomerization data, conditioned media from WT ANGPT1- and ANGPT1^{K249R}-expressing cells potently induced AKT phosphorylation, while media from ANGPT1^{Q236*}- or ANGPT1^{R494*}-expressing cells did not.

As ANGPT1^{K249R} was expressed and activated pAKT signaling normally, we used a pulldown approach to test its ability to interact with TEK (Figure 6C). Conditioned medium from HEK293 cells transfected with WT ANGPT1-FLAG or ANGPT1^{K249R}-FLAG was incubated with recombinant human TEK-Fc fusion protein comprising the TEK extracellular domain (Ala23-Lys745) tagged with a human IgG Fc sequence. Both WT ANGPT1 and ANGPT1^{K249R} were found to strongly bind TEK-Fc, confirming the ability of this variant protein to interact with its receptor.

The p.Q236* mutant cDNA did not produce a full-length intact protein with C-terminal FLAG tag, as the introduced stop codon is upstream of the tag sequence (Figure 6A and Supplemental Figure 7B). Therefore, to further analyze the function of the predicted protein product resulting from the p.Q236* mutation, we generated an additional ANGPT1^{Q236_F498del}-HA expression construct in which the HA tag was added in frame directly to the 3′ end of the predicted short ANGPT1^{Q236*} (M1-K235) protein. As ANGPT1^{Q236*} contains the intact ANGPT1 oligomerization domain (Figure 5B), we then performed immunoprecipitation assays to determine the

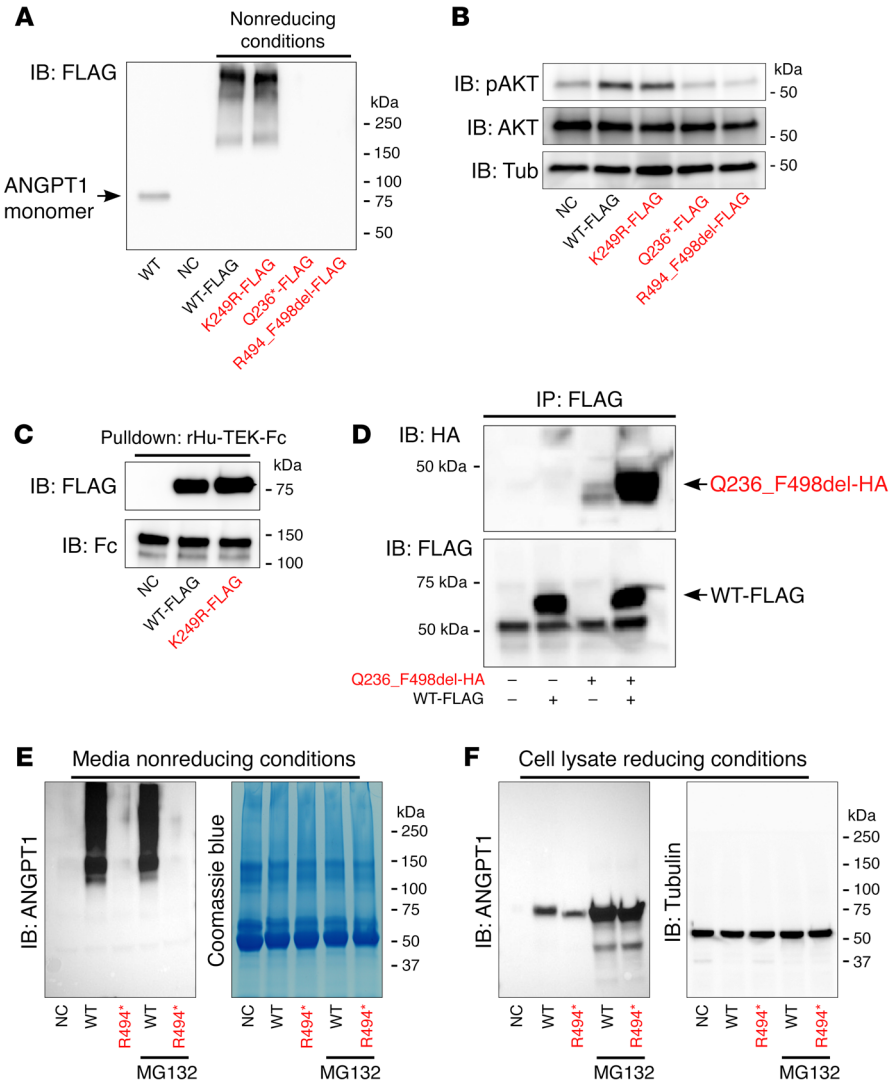

Figure 6. Expression and multimerization pattern of *ANGPT1* variants. (**A**) Western blot of FLAG-tagged WT and variant ANGPT1 proteins secreted by transfected HEK293 cells. Under nonreducing conditions WT and ANGPT1^{K249R} (K249R-FLAG) were observed in high-order oligomers. The premature stop codon upstream of the FLAG tag in ANGPT1^{Q236*} (Q236*-FLAG) prevented production of full-length, FLAG-tagged protein. Surprisingly, however, despite the insertion of the FLAG tag upstream of the premature stop codon in ANGPT1^{R494*} (R494_F498del-FLAG), no tagged protein was detected in the culture medium. (**B**) Western blot of HUVECs incubated with conditioned media from transfected HEK293 cells. Conditioned media from cells expressing WT ANGPT1 and ANGPT1^{K249R} strongly induced AKT phosphorylation, while media from cells expressing ANGPT1^{Q236*} and ANGPT1^{R494*} did not. (**C**) Conditioned medium from HEK293 cells transfected with WT ANGPT1-FLAG or ANGPT^{K249R}-FLAG was incubated with recombinant human TEK-Fc fusion protein to test the receptor-binding ability of this variant protein. (**D**) When coexpressed, FLAG-tagged WT ANGPT1 strongly pulled down ANGPT1^{Q236*} with an HA tag inserted upstream of the premature stop codon (Q236_F498del-HA), indicating an interaction and potential dominant-negative activity. (**E** and **F**) Untagged WT and R494* variant ANGPT1 was expressed in HEK293 cells and immunoblotted using anti-ANGPT1 antibody. Only WT protein was detected in the conditioned medium, while ANGPT1^{R494*} appears to be expressed but retained in the intracellular compartment. MG132 treatment was performed to block the proteasomal pathway. Coomassie blue staining and anti-tubulin (Tub) immunoblotting were used as loading controls for the conditioned media and cell lysate, respectively.

ability of this variant to oligomerize with WT ANGPT1 (Figure 6D). When coexpressed in HEK293 cells, ANGPT1^{Q236_F498del}-HA was found to robustly interact with WT ANGPT1. Although we expect the majority of *Angpt1*$^{p.Q236*}$ transcripts to be degraded by NMD, these results suggested that any ANGPT1^{Q236*} mutant protein that escapes NMD and is produced might act in a dominant-negative fashion by oligomerizing with WT ANGPT1 — diminishing TEK activation by forming ANGPT1 multimers with fewer receptor binding domains.

To exclude the possibility that protein trafficking or secretion defects we observed in cells transfected with ANGPT1^{R494*} were the result of expression tag addition, HEK293 cells were transfected with untagged WT *Angpt1* or *Angpt1*$^{p.R494*}$, and the conditioned media and cell lysates were subjected to SDS-PAGE (Figure 6, E and F). While WT ANGPT1 protein was observed in the cell media, ANGPT1^{R494*} was detected only in the cell lysate. Incubation with the proteasome inhibitor MG132 increased the abundance of both WT and mutant ANGPT1 within the cell, but had no effect on the secretion of mutant protein into the media. When observed by immunocytochemistry in transfected NIH 3T3 cells, WT ANGPT1 was distributed throughout the cell, only partially colocalized with an ER marker, protein disulfide isomerase (PDI; Figure 7A, top panel). However, unlike the uniform distribution of WT ANGPT1, ANGPT1^{R494*} was observed only in large vacuole-like structures that were colocalized with PDI (Figure 7A, bottom panel) but not Golgin-97 (a marker of the Golgi apparatus; Figure 7B). Taken together, these results suggested that ANGPT1^{R494*} was trapped within ER-derived vesicles and not secreted from the cell.

To determine whether ANGPT1^{R494*}, like ANGPT1^{Q236*}, could interact with WT ANGPT1 and act in a dominant-negative fashion, or whether the presence of WT ANGPT1 could aid in trafficking of the mutant protein, we cotransfected NIH 3T3 cells with WT ANGPT1-FLAG and untagged WT ANGPT1 or ANGPT1^{R494*}. Immunocytochemistry using anti-FLAG antibody revealed WT ANGPT1-FLAG in large intracellular vesicles when coexpressed with ANGPT1^{R494*}, but not with WT ANGPT1 (Figure 7B), suggesting that the mutant protein could interact with WT ANGPT1.

Generation and analysis of ANGPT1$^{p.R494*}$ *mutant mice.* In vitro, ANGPT1^{R494*} was not secreted and was instead found aggregated in ER-derived vesicles — consistent with our in silico analysis predicting that this variant would produce a strongly destabi-

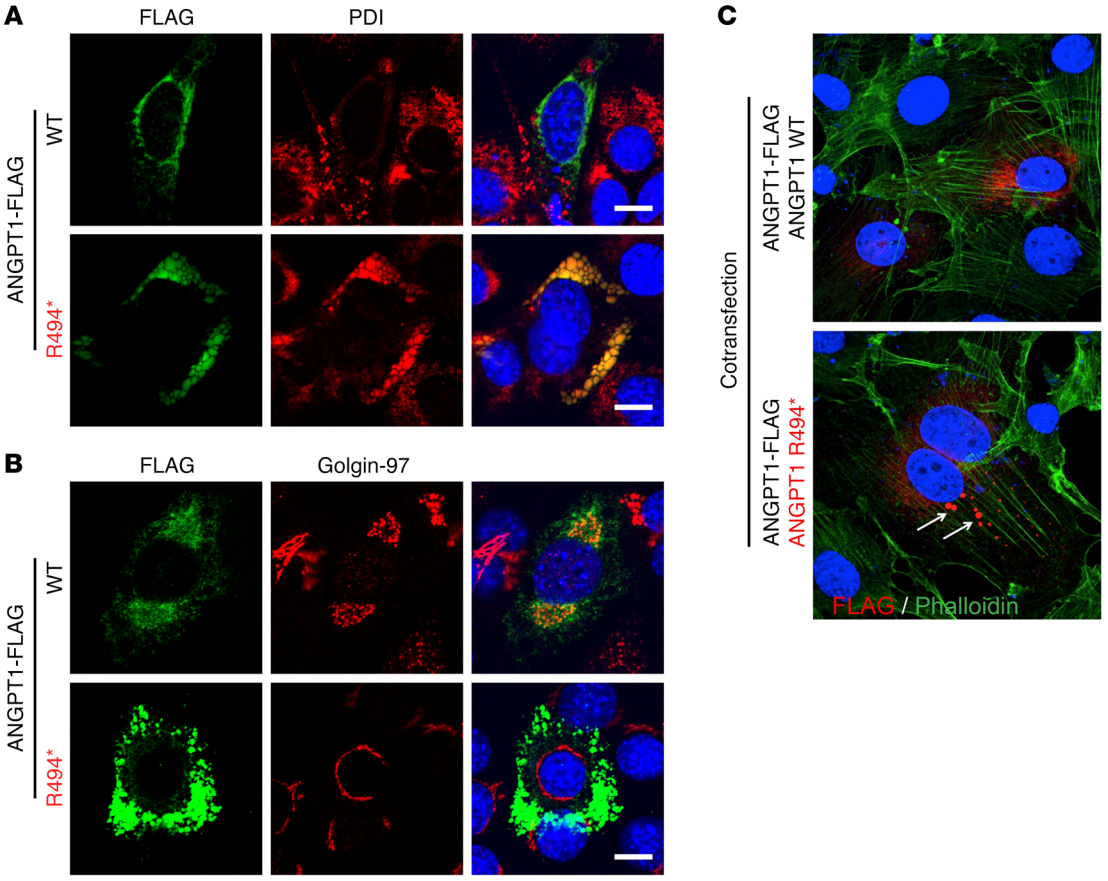

Figure 7. ANGPT1 p.R494* variant protein is trapped within intracellular aggregates. (**A** and **B**) Subcellular localization of WT and R494* variant ANGPT1. When expressed in NIH 3T3 cells, WT ANGPT1-FLAG detected using anti-FLAG antibody showed a staining pattern consistent with localization in the ER (**A**) and Golgi apparatus (**B**). However, ANGPT1^{R494*}-FLAG was observed aggregated in intracellular vesicles positive for the ER marker PDI but not Golgin-97, a marker of the Golgi apparatus. (**C**) Interaction between WT and ANGPT1^{R494*} within the cell. When coexpressed with untagged ANGPT1^{R494*}, FLAG-tagged WT protein detected with anti-FLAG antibody was trapped in intracellular aggregates (white arrows) with untagged ANGPT1^{R494*}. No WT ANGPT1-FLAG aggregates are observed in control cells coexpressing untagged WT ANGPT1. Scale bars: 10 μm.

lized protein. However, the critical oligomerization and receptor binding domains remained, and the effect of this variant on TEK signaling in vivo remained unclear. To investigate this variant protein in more detail, we therefore used a CRISPR/Cas9 genome-editing approach to generate a new mouse line carrying the p.R494* mutation (Figure 8, A and B). N1 offspring were born normally and genotyped by PCR (Figure 8C) and Sanger sequencing approaches (Figure 8D). Heterozygous pups were screened for off-target mutations (Supplemental Figure 8 and Supplemental Table 2) and used as founders for all subsequent experiments. Using reverse transcription PCR, *Angpt1*$^{p.R494*}$ mRNA was detected in E10.5 embryos, confirming that the modified transcript is produced and escapes NMD (Supplemental Figure 9). As we expected the *Angpt1*$^{p.R494*}$ allele to be loss of function, we additionally generated an *Angpt1*-null allele for purposes of comparison. This null allele was created by breeding of an *Angpt1*$^{WBΔE16.5}$ male with a WT female. Heterozygous *Angpt1*$^{Null/WT}$ mice were born normally and appeared healthy. We then generated litters of heterozygous *Angpt1*$^{p.R494*/WT}$ and *Angpt1*$^{Null/WT}$ mice with WT controls and analyzed SC development. At P14, SC exhibited normal morphology and PROX1 expression in both *Angpt1*$^{p.R494*/WT}$ and *Angpt1*$^{Null/WT}$ mice (Figure 8E). This finding was consistent with the normal IOP observed in adult *Angpt1*$^{Null/WT}$ heterozygous mice (Supplemental Figure 10).

Although the *Angpt1*$^{p.R494*}$ allele did not affect SC development in the heterozygous state, this lack of phenotype was shared by the *Angpt1* heterozygotes. Therefore, we set out to determine whether *Angpt1*$^{p.R494*}$ serves as a functional null allele in the absence of WT ANGPT1. As homozygous *Angpt1*^{Null} mice die between E9.5 and E12.5 (11, 12), an *Angpt1*$^{p.R494*/WT}$ heterozygous male mouse was crossed to *Angpt1*$^{Null/WT}$ and *Angpt1*$^{p.R494*/WT}$ females to generate litters of *Angpt1*$^{p.R494*/Null}$ compound mutants and *Angpt1*$^{p.R494*}$ homozygotes (Figure 9A). Strikingly, while *Angpt1*$^{p.R494*/Null}$ compound mutants were observed at E10.5 at normal Mendelian ratios (Figure 9A), no *Angpt1*$^{p.R494*/Null}$ compound mutants or *Angpt1*$^{p.R494*/p.R494*}$ homozygotes were found alive by E12.5, and no mutants were observed in litters collected after birth — demonstrating that the *Angpt1*$^{p.R494*}$ mutant allele is functionally null.

At E10.5, whole-embryo CD31 staining showed that the majority of p.R494*/Null compound-mutant embryos appeared normal, with similar vascular patterning to control littermates. However, some embryos appeared smaller with disorganized vasculature reminiscent of that reported in ANGPT1-null mice (Fig-

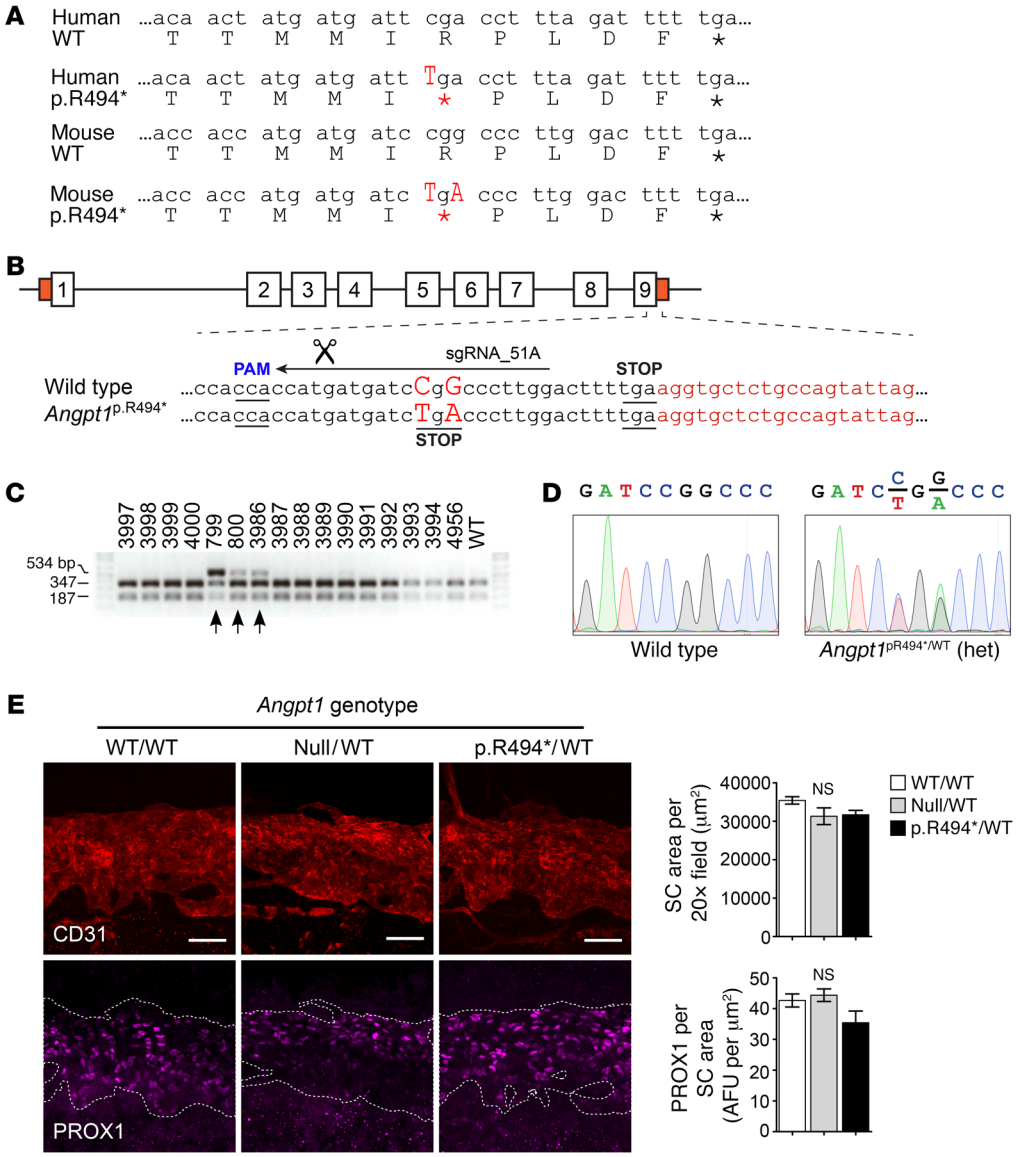

Figure 8. Generation and analysis of *Angpt1*$^{p.R494*}$ mice. (**A**) The CRISPR/Cas9 system was used to generate a novel ANGPT1^{R494*}-expressing mouse line. While Arg-494 is conserved between mice and humans, it is encoded by different codons in each species. Therefore, different genomic DNA modifications are required for the p.R494* substitution in mice and humans. (**B**) Targeting strategy used to design guide RNAs. (**C**) Genotyping of N1 mice showing positive mutants following PCR and *HpaII* digestion. (**D**) Sanger sequencing analysis of a heterozygous founder mutant. (**E**) SC appears normal in *Angpt1*$^{Null/WT}$ and *Angpt1*$^{p.R494*/WT}$ heterozygous mice. In **E**, n = 3 WT/WT, 3 Null/WT, and 5 p.R494*/WT (SC area) or 3 (PROX1 expression) animals per group. Scale bars: 50 μm; ×20 fields comprise an area of 65,536 μm².

ure 9B and ref. 12). By E12.5, all *Angpt1*$^{p.R494*/Null}$ compound mutants and *Angpt1*$^{p.R494*/p.R494*}$ homozygotes were deceased, and some were in the process of being reabsorbed (*Angpt1*$^{p.R494*/Null}$, 2 of 5; *Angpt1*$^{p.R494*/p.R494*}$, 5 of 6; Figure 9, B and C). While most embryos were degraded and not available for analysis, some had visible symmetrical hemorrhage in the region of the jugular lymph sacs.

As homozygous *Angpt1*$^{p.R494*/p.R494*}$ embryos die in utero, we were unable to examine the effect of this variant on SC development in the homozygous state. Instead, we crossed heterozygous *Angpt1*$^{p.R494*/WT}$ animals with *Angpt1*-inducible knockouts to generate a new *Angpt1*$^{p.R494*/fl}$ *Rosa26*^{rtTA} TetOnCre strain (*Angpt1*$^{p.R494*/Δ}$ mice). By administering doxycycline to these mice at E16.5, we excised the *Angpt1*^{fl} allele and obtained viable pups expressing only ANGPT1$^{p.R494*}$ (*Angpt1*$^{p.R494*/ΔE16.5}$). As predicted, when SC morphology was examined at P21, *Angpt1*$^{p.R494*/ΔE16.5}$ mice were found to have a hypomorphic SC phenotype with reduced PROX1 expression — duplicating the phenotype observed in *Angpt1*$^{WBΔE16.5}$ mice and confirming that ANGPT1$^{p.R494*}$ cannot replace WT ANGPT1 in SC development (Figure 10).

Discussion

Angpt1;Angpt2 double-knockout mice rapidly develop a severe glaucoma phenotype, characterized by complete lack of SC, buphthalmos, markedly elevated IOP, and severe damage to the neural retina (7). This phenotype is replicated in mice lacking the angiopoietin receptor TEK, confirming that signaling through the classical angiopoietin/TEK signaling axis is essential for SC formation (7, 8). However, while the importance of TEK signaling is clear, specific roles for each angiopoietin ligand have not been previously described. Here, we identify a critical role for ANGPT1 in development of SC and describe 2 PCG patients carrying heterozygous loss-of-function mutations in the *ANGPT1* gene.

Mice lacking ANGPT1 alone, or both ANGPT1 and ANGPT2, failed to form a normal SC and rapidly developed ocular hypertension. However, as the phenotype of *Angpt1;Angpt2* double knockouts was more severe than that observed in knockouts of *Angpt1* alone, we hypothesize that although the proteins have canonically opposing roles, compensation between angiopoietin ligands was occurring in SC. Unlike the well-defined agonistic

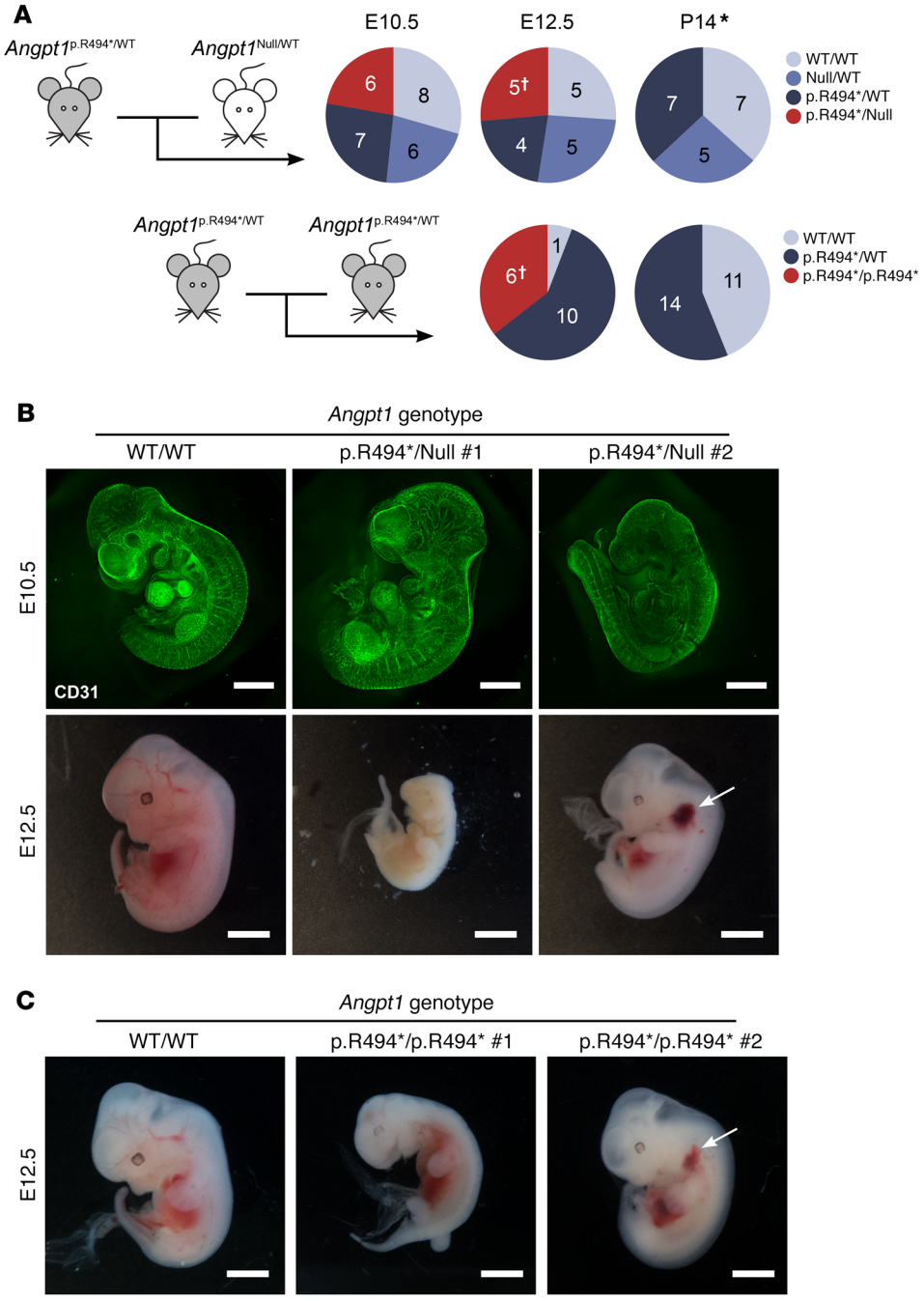

Figure 9. *Angpt1*$^{p.R494*}$ cannot replace WT *Angpt1* in embryonic development. (**A**) Heterozygous *Angpt1*$^{p.R494*/WT}$ mice were crossed with *Angpt1*$^{Null/WT}$ animals or inbred with *Angpt1*$^{p.R494*/WT}$ mice to generate p.R494*/Null or p.R494*/p.R494* offspring completely lacking WT ANGPT1 protein. While *Angpt1*$^{p.R494*/Null}$ pups were observed at normal Mendelian ratios early in embryonic development, double-mutant and homozygous mutant embryos died between E10.5 and E12.5 and no viable pups were born. (**B** and **C**) At E10.5, while all embryos were found alive, some *Angpt1*$^{p.R494*/Null}$ double mutants appeared smaller than control littermates and exhibited disorganized vasculature. By E12.5, all double-mutant and p.R494* homozygous embryos were found deceased (**B** and **C**), and some had been partially reabsorbed. Interestingly, some embryos had a visible hemorrhage in the region of the jugular lymph sac (white arrows), suggesting a possible defect in lymphovenous valve function. †Pups found deceased. *No mortality was observed between birth and P14. Scale bars: 1 mm (**B**, top panels) and 2 mm (**B**, bottom panels, and **C**).

behavior of ANGPT1, the role of ANGPT2 remains poorly understood. It has been described as a context-dependent TEK agonist/antagonist or weak agonist, but there is no consensus as to the cues mediating signaling activity in different endothelial beds. The ligandless receptor TIE (also known as TIE1) (22), integrins (23, 24), and level of TEK expression (23) have been proposed as factors mediating ANGPT2's different roles. Classic experiments on the ANGPT1-mediated rescue of intestinal lacteals in an *Angpt2*-knockout model confirm the ability of ANGPT2 to act as a TEK agonist in the lymphatic endothelium (14). However, this compensation did not occur in the retinal blood vasculature, indicating a clear difference between the roles of ANGPT2 in the blood and lymphatic endothelium.

Here, we have identified the alternate situation in vivo, as ANGPT2 compensates for the lack of ANGPT1 in the unique SC endothelium. Despite the lack of an apparent SC phenotype in *Angpt2*-knockout eyes, a clear difference was apparent between the eyes of *Angpt1*- and *Angpt1*;*Angpt2*-knockout animals. This finding suggests a compensatory role for ANGPT2 in the absence of the primary TEK ligand ANGPT1. Lacking adequate ANGPT1, ANGPT2 provides partial compensation, allowing limited canal formation (Figure 11A).

The developmental failure of SC in *Angpt1*-knockout mice appears to occur through 2 separate but related processes: reduced sprouting from the LVPs, and decreased proliferation of the vascular sprouts that form SC. Unlike VEGF signaling, which acts

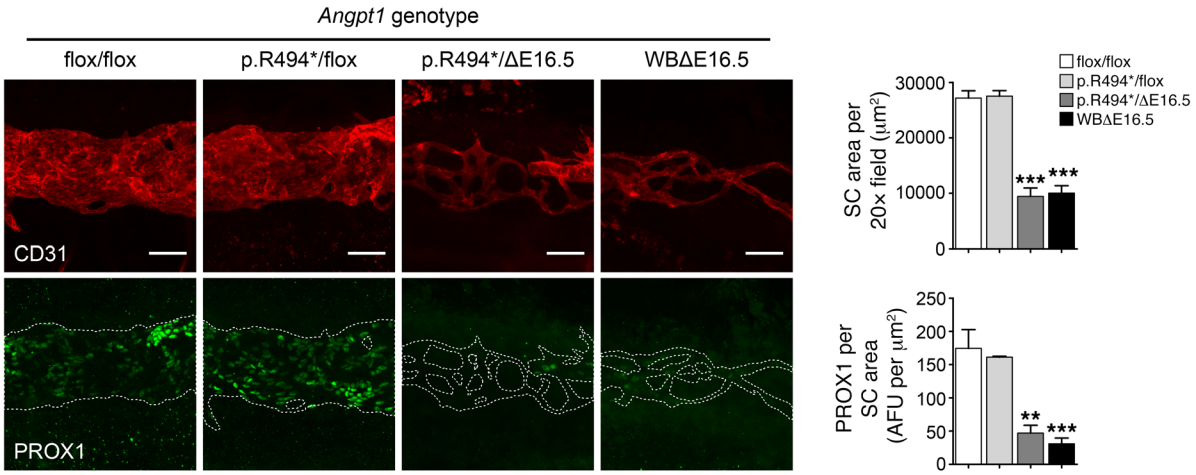

Figure 10. *Angpt1*$^{p.R494*}$ cannot replace WT *Angpt1* in SC development. Compared with littermate flox/flox and p.R494*/flox controls, at P21, *Angpt1*$^{p.R494*/\Delta E16.5}$ mice exhibited a hypomorphic SC with reduced PROX1 expression resembling that of *Angpt1*$^{WB\Delta E16.5}$ mice. This finding confirms that the *Angpt1*$^{p.R494*}$ allele is functionally null in the context of SC development. n = 5 (flox/flox), 3 (p.R494*/flox and p.R494*/ΔE16.5), and 8 (WBΔE16.5) animals per group. $^{**}P < 0.01$, $^{***}P < 0.001$ vs. flox/flox as determined by 1-way ANOVA followed by Bonferroni's correction. AFU, background subtracted arbitrary fluorescence units. Scale bars: 50 μm; ×20 fields comprise an area of 65,536 μm^2.

predominantly to encourage endothelial sprouting, ANGPT1-mediated TEK activation has been described to have a critical role in vascular stability and regulation of venous diameter, and cannot directly initiate sprouting angiogenesis (25). However, ANGPT1 can increase the sprouting angiogenic response to VEGF (26), and as VEGF signaling is essential for the initial sprouting in SC development (5), our data suggest that ANGPT1 has a similar potentiating effect in the canal. Angiogenic sprouts leave the blood vascular plexuses of the limbus and are drawn into the limbal tissue toward the iridocorneal angle, probably by a gradient of VEGF (5, 6). In the absence of ANGPT1 this proangiogenic stimulus was reduced, blunting the sprouting process. As pre-SC endothelial cells must interact with neighboring sprouts in order to consolidate and form the mature canal (5), we hypothesize that the reduced sprouting observed in *Angpt1*-knockout mice was directly related to the failure of canal formation. With fewer sprouts available for interaction, fewer cells find their neighbors to begin the process of canal development. It is possible that the infrequent interactions that do occur in *Angpt1*-knockout mice are responsible for the isolated canal segments we observed, suggesting a direct link between efficiency of the initial sprouting process and eventual aqueous humor drainage function (Figure 11B).

In addition to the reduction in endothelial sprouts observed in the *Angpt1* knockout, the failure of the narrow, disorganized primordial SC to widen into a mature vessel is reminiscent of the role ANGPT/TEK signaling plays in venous widening (25). In patients, *TEK* mutations that cause hyperactivation of the receptor lead to an extreme version of this effect, resulting in hereditary and sporadic venous malformations (27, 28). SC has been described as a "hybrid vessel," incorporating elements of both blood and lymphatic vascular physiology (4–7, 29, 30). However, it can perhaps be most accurately described as a large vein-like structure that expresses the lymphatic transcription factor PROX1 in addition to classical venous markers such as endomucin, CD34, and COUP-TFII (Supplemental Figure 11 and refs. 4–6). Just as treatment with recombinant ANGPT1 is sufficient to cause venous enlargement in the microvasculature of the dermis and trachea (25), our results indicate that native ANGPT1 signaling in the iridocorneal angle is required for proliferation and widening of the venous-lymphatic hybrid SC endothelium from a narrow sprouting plexus into its mature form.

Interestingly, although the SC defects we observed are caused by loss of an endothelial-specific growth factor pathway, the TM of *Angpt1*-knockout mice was found to be severely hypoplastic, suggesting a critical role for SC endothelium in regulation of TM development. A similar mechanism is well described in other endothelial beds, such as the renal glomerulus, where PDGFB signaling from the glomerular endothelium is critical for recruitment of mesangial cells (31).

The importance of ANGPT1 in the development and maintenance of aqueous humor homeostasis is confirmed by the discovery of rare *ANGPT1* loss-of-function mutations in our cohort of PCG patient families. Consistent with the results of our mouse genetics studies, no PCG-associated variants were discovered in the *ANGPT2* or *ANGPT4* genes, emphasizing the role of ANGPT1 as the dominant TEK ligand in SC. Interestingly, while both novel *ANGPT1* nonsense mutations we identified have a clear impact on ANGPT1 function and its ability to interact with the TEK receptor, each has a different mechanism. p.Q236* completely lacks the C-terminal receptor binding domain, which is required for interaction with TEK (19, 20). In addition, the truncated ANGPT1^{Q236*} protein can readily form oligomeric complexes through its intact N-terminal domain with WT ANGPT1, a process that is critical to the signaling function of ANGPT1 (18, 19). We hypothesize that in heterozygous PCG patients, any truncated protein that escapes NMD might have a dominant-negative function on ANGPT1 signaling.

Compared with p.Q236*, the impact of the p.R494* mutation on ANGPT/TEK signaling was more difficult to predict, as the mutant protein lacked only 5 amino acids at the C-terminus, located outside of the receptor binding surface. Nevertheless,

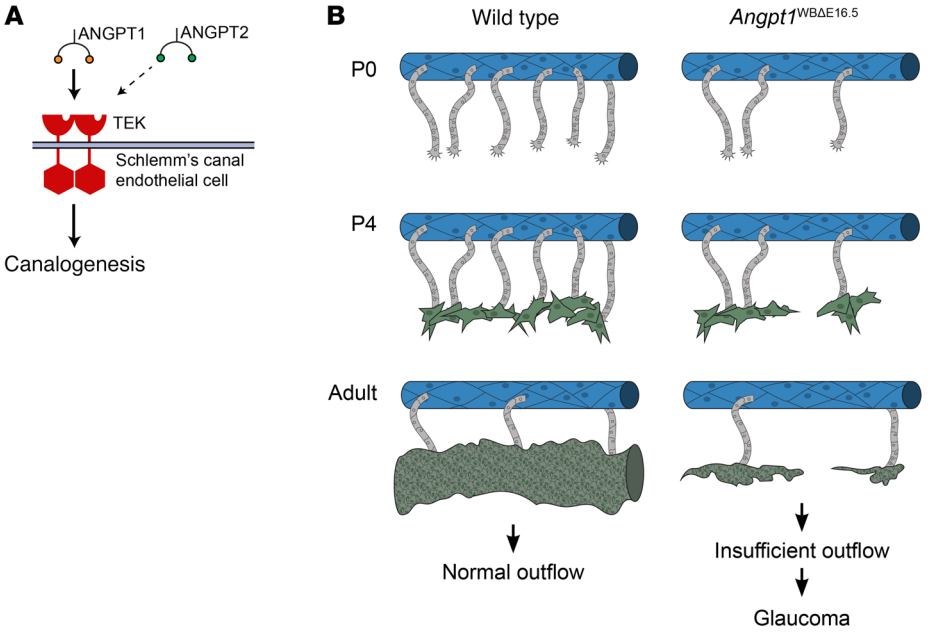

Figure 11. Defects in ANGPT/TEK signaling result in a hypoplastic SC insufficient for normal drainage. (**A**) ANGPT1 is the primary TEK ligand in SC development, although limited compensation from ANGPT2 is possible. (**B**) Reductions in ANGPT1/TEK signaling lead to reduced angiogenic sprouting from the superficial vascular plexus (blue). The sparse sprouts observed in *Angpt1*$^{WBΔE16.5}$ mice are unable to reach their neighbors, interdigitate, and mature into a normal SC (green), resulting in irregular canal formation, inadequate aqueous humor drainage, and glaucoma.

these residues are highly evolutionarily conserved, and in silico analysis tools predicted that this mutation would strongly destabilize the folded protein. Consistent with these predictions, our in vitro studies revealed that ANGPT1^{R494*} was unable to be secreted due to its retention within intracellular ER-derived vesicles. When coexpressed, WT ANGPT1 was also trapped in these vesicles, indicating that, like ANGPT1^{Q236*}, the ANGPT1^{R494*} variant protein product may also have a dominant-negative effect on ANGPT signaling in the heterozygous state.

Both p.Q236* and p.R494* variants displayed potential dominant-negative effects in our in vitro assays. However, as ANGPT1 is essential for development of the embryonic cardiovascular system, any dominant-negative variant compatible with life must have an incomplete effect. In the case of the p.Q236* variant, this may be explained by nonsense-mediated decay of the variant transcript. Even if the truncated protein was strongly dominant negative, we predict that it would be expressed at low levels compared with the WT allele in heterozygous patients. However, interindividual variability has been reported in NMD efficiency, and this may result in variable penetrance of disease in affected patients (32). Similarly, while the p.R494* variant displayed potential dominant-negative effects in our in vitro analysis, this effect was minimal or absent in vivo. ANGPT1 signaling is essential for embryonic vascular development, and *Angpt1*-null mice die between E9.5 and E12.5 (11, 12). However, *Angpt1*$^{p.R494*/WT}$ heterozygous mice were born normally with a normal SC — indicating that sufficient ANGPT/TEK signaling was present to allow vascular development. Despite this minimal or absent dominant-negative effect, ANGPT1^{R494*} was unable to replace WT ANGPT1 in mouse vascular development, and *Angpt1*$^{p.R494*/Null}$ compound mutant or *Angpt1*$^{p.R494*/p.R494*}$ homozygous mice did not survive until birth, dying between E10.5 and E12.5. At E10.5, some compound mutant embryos appeared smaller than healthy controls, with profoundly disturbed vascular patterning. A similar finding has been reported in *Angpt1* full-body-knockout mice, confirming that *Angpt1*$^{p.R494*/Null}$ and *Angpt1*$^{p.R494*/p.R494*}$ mice are functionally analogous to full *Angpt1* knockouts.

Although heterozygous *Angpt1*$^{p.R494*/WT}$ mice did not display SC defects, we have previously shown that TEK heterozygosity in mice results in comparatively minor defects in SC morphology and only slightly elevated IOP. However, in patients, the defect is much more severe, leading to PCG with dramatic IOP elevation (>10 mmHg), buphthalmos, and optic neuropathy (8). This suggests a greater sensitivity to ANGPT/TEK signaling defects in the human eye compared with the mouse, and we hypothesize that any defect or haploinsufficiency in ANGPT/TEK signaling has a pathogenic effect in human patients with variable expressivity.

The third *ANGPT1* variant identified in our PCG cohort, p.K249R, is a rare missense allele observed only once, in a South Asian individual, in the ExAC exome variant database. Despite the strong evolutionary conservation of K249 and its location within the critical multimerization domain, we were unable to identify defects in oligomerization, secretion, receptor binding ability, or downstream signaling by this variant protein using our in vitro system. While p.K249R may have an effect on ANGPT1 signaling function that was undetected using our system, without additional information about disease and genotype segregation in this family we cannot exclude the possibility that this patient carries an unidentified mutation in another gene responsible for the disease. Furthermore, the p.K249R subject identified in our PCG cohort is of Kenyan descent, a population that is underrepresented in ExAC and other public databases, raising the possibility that p.K249R is a population-specific benign variant.

In summary, discovery of pathological *ANGPT1* mutations in PCG families implicates a second member of the ANGPT/TEK signaling axis in glaucoma pathogenesis and underscores the importance of this signaling system in the function of the anterior segment of the human eye. Importantly, unlike the known PCG-associated genes *CYP1B1*, *LTBP2*, *FOXC1*, and *MYOC*, the ANGPT/TEK pathway offers a number of proteins that might be targeted by potential therapies in the future. The range of IOP and SC morphological phenotypes observed in mice deficient in TEK signaling demonstrates the exquisite balance of signaling events

in canalogenesis and highlights the pharmacological potential of TEK-modulating therapy in patients with decreased aqueous humor outflow or ocular hypertension.

Methods

Generation and breeding of inducible, whole-body angiopoietin-knockout mice. Inducible, whole-body deletion of *Angpt1* and *Angpt2* was achieved using a reverse-tetracycline-controlled transactivator (rtTA) system driven by the ubiquitously expressed *Rosa26* promoter in combination with *Angpt1* and *Angpt2* floxed alleles as previously described (7, 12, 33). Timed, whole-body excision was induced by addition of doxycycline hyclate (0.5%; Sigma-Aldrich) to the drinking water. All mice described in this study were given doxycycline at E16.5, and doxycycline treatment was continued until P14 or dissection (if earlier). Flox/flox littermate mice lacking the rtTA transgene, and thus protected from doxycycline-mediated Cre recombinase expression, were used as controls throughout the study. Animals were given unrestricted access to standard rodent chow (Harlan; no. 7912) and water. All mice were kept on a mixed genetic background, and animals of both sexes were included in comparisons. Knockout mice were genotyped by PCR, using the following primers: *Angpt1*^{fl}, forward 5′-CAATGCCAGAGGTTCTTGTGAA-3′, reverse 5′-TCAAAGCAACATATCATGTGCA-3′ (WT, 233-bp product; *Angpt1*^{fl}, 328 bp); *Angpt1*^{delete}, forward 5′-CAATGCCAGAGGTTCTTGTGAA-3′, reverse 5′-TGTGAGCAAAACCCCTTTC-3′ (431-bp product); *Angpt2*^{fl}, forward 5′-GGGAAACCTCAACACTCCAA-3′, reverse 5′-ACACCGGCCTCTAGACACAC-3′ (WT, 224-bp product; *Angpt2*^{fl}, 258 bp); and *Angpt2*^{delete}, forward 5′-AAGGCGCATAACGATACCAC-3′, reverse 5′-TGAGAACTCTGCAGCCTTGA-3′ (*Angpt2*^{fl}, 1,372-bp product; *Angpt2*^{delete}, 426 bp).

Real-time PCR. *Angpt1* and *Angpt2* deletion was confirmed using quantitative, real-time PCR. Lung tissue from whole-body knockout mice was collected, and total RNA was isolated using Trizol reagent (Life Technologies). cDNA was then generated using the iScript kit (Bio-Rad Laboratories), and real-time PCR was performed on an ABI 7500 thermocycler (Applied Biosystems) using iTaq SYBR Green master mix (Bio-Rad Laboratories) and the following primers: *Gapdh*, forward 5′-AAGGTCATCCCAGAGCTGAA-3′, reverse 5′-CTGCTTCACCACCTTCTTGA-3′; *Angpt1*, forward 5′-GGGGGAGGTTGGACAGTAA-3′, reverse 5′-CATCAGCTCAATCCTCAGC-3′; *Angpt2*, forward 5′-GATCTTCCTCCAGCCCCTAC-3′, reverse 5′-TTTGTGCTGCTGTCTGGTTC-3′.

Human study participants. PCG was defined by the following characteristics: (a) age of onset less than 3 years, (b) increased corneal diameter greater than 10 mm accompanied by corneal edema and/or Haab's striae, and (c) IOP greater than 21 mmHg and/or optic nerve cupping greater than 0.4. Any patient with other ocular abnormalities or systemic conditions, other than iris stromal hypoplasia, was excluded from the study. Subjects and their families were recruited from multiple international centers, each of which had received study approval from its respective IRB. Our studies adhered to the tenets of the Declaration of Helsinki and were compliant with the Health Insurance Portability and Accountability Act (HIPAA).

Exome and Sanger sequencing. Exome sequencing of 135 PCG families was performed using Nimblegen EZ version 3 (Roche) or SureSelect V4/V5 (Agilent) capture kits, and 2 × 100-bp paired-end sequencing on a HiSeq2500 platform (Illumina). Reads were aligned to the human reference genome (GRCh37/hg19) using the Burrows-Wheeler Aligner (BWA) (http://bio-bwa.sourceforge.net/), and duplicates were marked and removed using Picard (http://broadinstitute.github.io/picard/). Single-nucleotide variants and small insertions/deletions (indels) were called using Genome Analysis Toolkit (GATK; Broad Institute) and annotated against RefSeq transcripts using ANNOVAR. Variant data were filtered to remove synonymous changes, intronic variants more than 10 nucleotides from the intron-exon splice site junctions, variants present in the ExAC public database (exac.broadinstitute.org) at an allele frequency greater than 0.0001, and variants identified in an in-house database of 120 control exomes. All exome variants identified in *ANGPT1* were validated by Sanger sequencing. The *ANGPT1* gene was also directly Sanger-sequenced in an additional 80 PCG families. Genomic primer sequences are provided in Supplemental Table 3.

Design and generation of the ANGPT1^{R494*} *mutant mouse line*. A CRISPR/Cas9 approach was used to generate ANGPT1^{R494*} mice. While the protein sequence flanking R494 is conserved in humans and mice, R494 is encoded using different codons (Figure 8A). Therefore, the genomic mutation used to generate p.R494* mice (c.1477C>T; c.1479G>A) is slightly different from that observed in human patient family 1 (c.1480C>T). To generate this mutation, a Web-based CRISPR design tool (http://crispr.mit.edu/) was used to select candidate guide RNA sequences and scan for possible off-target matches throughout the mouse genome. Five candidate single-guide RNA (sgRNA) sequences were selected for testing (Supplemental Table 1). Selected sgRNAs were cloned into the pX458 vector (Addgene plasmid 48138), which expressed SpCas9 in mammalian cells. sgRNA activity was validated in mouse Neuro-2a cells (Sigma-Aldrich) before injection as previously described (34). For zygote injection, sgRNA 5.1_sgRNA (Figure 8B) was selected and in vitro–transcribed and purified using the MEGAshortscript (AM1354) and MEGAclear kits (AM1908) from Ambion (Life Technologies). We injected Cas9 mRNA (GeneArt CRISPR Nuclease mRNA catalog A29378), sgRNA, and single-stranded oligonucleotide (chemically synthesized and desalted ssODN; Integrated DNA Technologies) into the cytoplasm of single-cell fertilized C57BL/6J zygotes (The Jackson Laboratory). Litters of N1 pups were obtained and screened for positive mutants by PCR and Sanger sequencing. Genomic DNA was prepared from a tail biopsy using standard methods, and a PCR product flanking the mutated region was prepared using the following primers: forward 5′-TCCCTTCCTCTGGTTACACG-3′, reverse 5′-AAGTGGCGATTCTGTTGACC-3′. Mutants were identified by digestion of PCR product using *HpaII* (Figure 8C), and positive individuals were confirmed by Sanger sequencing (Figure 8D). The MIT CRISPR design tool (http://crispr.mit.edu/) was used to obtain a list of possible off-target mutation sites (Supplemental Table 2), and Sanger sequencing was used to confirm a lack of off-target mutations in the 5 strongest matches (Supplemental Figure 8).

Live-animal studies. IOP was measured using a Tonolab rebound tonometer (iCare Finland) as previously described (7, 35). Animals were restrained in a soft plastic cone, and average IOPs were recorded from 3 sets of 6 recordings performed by a blinded technician. Finding no difference between left and right eyes, we have reported all IOP measurements as single averaged values for each animal.

Whole-mount immunostaining. Eyes were enucleated and immersion-fixed overnight at 4°C (2% formaldehyde in PBS, pH 7.5). After fixation, eyes were bisected on the sagittal plane, lens and retina were removed, and eyes were stained as whole mounts for confocal micros-

copy. Retinal ganglion cells were visualized in retina flat mounts as previously described (36).

Fixed tissues were blocked overnight at 4°C (5% donkey serum, 2.5% BSA, 0.5% Triton X-100 in TBS, pH 7.5). After blocking, samples were incubated overnight in appropriate blocking buffer–diluted primary antibodies. The following primary antibodies and dilutions were used: rat anti–mouse CD31 (BD Pharmingen; 550274; 1:100), goat anti–human PROX1 (R&D Systems; AF2727; 1:250), rabbit anti–mouse Ki67 (Thermo Fisher Scientific; MA5-14520; 1:250), rat anti–mouse endomucin (Abcam; AB106100; 1:250), goat anti–mouse LYVE-1 (R&D Systems; AF2125; 1:250), rat anti–mouse CD34 (BD Pharmingen; 553731; 1:500), rabbit anti–human vWF (Dako; A0082; 1:1,000), mouse anti-Brn3a (Millipore; MAB1585; 1:400), goat anti-Brn3b (Santa Cruz Biotechnology; sc-6026; 1:1,000). Eyes were washed at room temperature (6 × 1 hour, 0.05% Tween-20 in TBS, pH 7.5) and returned to 4°C for overnight incubation in appropriate Alexa Fluor–labeled secondary antibodies (Invitrogen). After staining, tissues were washed a second time before trimming and mounting. Tissues were imaged using a Nikon A1R confocal microscope at the Center for Advanced Microscopy of Northwestern University. Images of SC development were captured using a ×20 objective with a numerical aperture of 0.75 to collect 10-image Z-stacks with a step size of 1.67 μm and a pinhole of 1.2 Airy units. Images are shown in the figures as maximum-intensity projections generated using Fiji software (37). Image quantification of whole-mounted limbal regions was performed by capturing of 3 images at intervals from each eye. Measurements from these replicates were averaged to obtain final values for each animal. Large-field images of adult SC morphology were obtained by stitching of images captured using the same ×20 objective and a fully opened 150-μm pinhole.

Whole-mount embryo analysis. Embryos from *Angpt1*$^{p.R494^*}$ mutant mice were collected at E10.5 and fixed (2% formaldehyde in PBS, pH 7.5, overnight at 4°C). Fixed embryos were then embedded in acrylamide hydrogel (4% acrylamide, 0.25% bis-acrylamide in PBS, pH 7.5) containing a thermal initiator [0.25%; Wako Chemicals; 2,2-AZO-BISY2-(2-IMIDAZOLAN-2)]. After overnight incubation at 4°C to allow acrylamide penetration, samples were moved to 37°C for 4 hours to polymerize the hydrogel. Samples were then blocked and stained with anti-CD31 antibodies as described above and mounted using sorbitol-based refractive index matching solution (70% sorbitol (w/v) in 0.02 M phosphate buffer pH 7.5 containing 0.01% sodium azide) (36). Mounted embryos were imaged using a Nikon A1R confocal microscope. Stitched 10-image *Z*-stacks are presented in the figures as maximum-intensity projections. Larger embryos (>E10.5) were collected and imaged using a Panasonic Lumix digital camera.

TM analysis. Semithin sections of the iridocorneal angle and TM were prepared and stained as previously described (8, 38). For α-smooth muscle actin staining, enucleated eyes were immersion-fixed as described above before dehydration and paraffin embedding according to standard methods. Five-micrometer sections were prepared and dewaxed, and antigen retrieval was performed (10 mM Tris, 1 mM EDTA, 0.05% Tween-20, pH 9, autoclaved 121°C 30-minute liquid cycle) before blocking (5% donkey serum, 2.5% BSA, 0.5% Triton X-100 in TBS, pH 7.5, 1 hour at room temperature) and overnight incubation with FITC-conjugated primary antibody (Sigma-Aldrich; F3777; 1:250). After staining, slides were mounted and imaged on a Nikon C2+ confocal microscope.

Reporter mouse lines. *Angpt1*^{GFP} (*Angpt1*$^{tm1.1Sjm/J}$) mice were a gift from Sean Morrison (University of Texas Southwestern Medical Center, Dallas, Texas, USA) and were generated and genotyped as previously described (39). Adult eyes were collected, fixed as described above, and embedded in OCT media for cryosectioning. Ten-micrometer cryosections were collected, blocked as described above, and stained using anti-GFP (Thermo Fisher Scientific; PA5-22688, 1:500) and anti-endomucin (Abcam; Ab106100; 1:250) antibodies. *Angpt2*^{LacZ} (*Angpt2*^{tm1Gdy}) mice were generated and genotyped as previously described (14). After collection, eyes were briefly fixed (0.2% glutaraldehyde in PBS, pH 7.4), washed (TBS containing 0.05% Tween-20), and incubated overnight in 1 mg/ml X-gal staining solution at 37°C. After staining, eyes were fixed overnight in 10% formalin before paraffin embedding and sectioning using standard methods. *Prox1*-tdTomato [Tg(Prox1-tdTomato)] mice were a gift from Guillermo Oliver (Northwestern University Feinberg School of Medicine, Chicago, Illinois, USA) and were genotyped as previously described (40). Adult eyes were used for whole-mount immunostaining as described above.

In vitro assays. HEK293 and NIH 3T3 cells were gifts from Tomoko Hayashida (Northwestern University Feinberg School of Medicine). HUVEC-C cells (CRL-1730) were purchased from the ATCC. ANGPT1 expression constructs were created by cloning of full-length ANGPT1 cDNA into the pcDNA3 vector. 3′-FLAG (DYKDDDK) or -HA (YPYDVPDYA) tag sequences were introduced replacing the stop codon in frame using standard cloning methods (Supplemental Figure 7). To introduce mutations into this WT *ANGPT1* vector, site-directed mutagenesis was performed using the PrimeSTAR Max kit (Takara Bio Inc.) to generate variant ANGPT1-expressing vectors.

Western blot analysis. Intracellular and secreted ANGPT1 protein abundance was determined by Western blot. Plasmid vectors containing variant or WT ANGPT1 were transfected into subconfluent HEK293 cells seeded in 6-well culture dishes using Lipofectamine 2000 reagent (Life Technologies). The following day, the cells were transferred to serum-free media and incubated for 24 hours before harvesting by lysis in 2× Laemmli sample buffer. Conditioned growth media were collected and concentrated using a size-filter exclusion column (Amicon Ultra; 10 kDa; Merck Millipore). Concentrated media were then diluted with sample buffer. For reducing conditions, β-mercaptoethanol was added. Samples were separated by SDS-PAGE and transferred to PVDF membranes using standard procedures before protein abundance was detected using mouse anti–human ANGPT1 (R&D Systems; MAB9231; 1:500) and mouse anti–FLAG M2 (Sigma-Aldrich; F3165; 1:5,000) antibodies. For loading control of cell lysates, α-tubulin was detected using anti–α-tubulin antibody (clone DM1A, catalog 32293; Santa Cruz Biotechnology; 1:2,000). For loading control of conditioned media, membranes were stained using GelCode Blue reagent (Bio-Rad Laboratories). For the proteosomal inhibitor study, transfected HEK293 cells were treated with 1 μM MG132 (Enzo Life Sciences) or DMSO for 24 hours.

TEK-Fc pulldown assay. The interaction of ANGPT1 and TEK receptor was tested as follows. WT and mutant ANGPT1 proteins were produced by transfection of HEK293 cells with expression vectors encoding FLAG-tagged variant proteins as described above. Conditioned medium was collected and mixed with 1 μg of recombinant human TEK2-Fc protein (Ala23-Lys745; R&D Systems; 313-TI-100) and incubated for 1 hour. Then, protein A beads blocked with 5% BSA solution were added to the medium to capture TIE2-Fc/ANGPT1

complexes. Samples were washed with TBS with 0.1% Triton X-100 and eluted with Laemmli sample buffer containing β-mercaptoethanol. The presence of ANGPT1-TEK-Fc complexes was determined by Western blotting using antibodies against FLAG and human IgG.

HUVEC stimulation assay. The ability of mutant ANGPT1 proteins to activate TEK downstream signaling was performed as follows. Conditioned media from HEK293 cells transfected with WT or mutant ANGPT1 proteins were prepared as described above for the TEK-Fc pulldown assay. After harvesting of conditioned medium, it was concentrated using a size-exclusion column (Amicon Ultra; 10 kDa). HUVECs were stimulated with concentrated conditioned media for 30 minutes at 37°C and then harvested by lysis in 2× Laemmli sample buffer.

Immunocytochemistry. Intracellular ANGPT1 distribution was determined by immunocytochemistry. NIH 3T3 cells were seeded onto coverslips coated with 0.1% poly-L-lysine (Sigma-Aldrich). Subconfluent cells were transfected with variant or WT ANGPT1-expressing vectors using Lipofectamine 2000. Transfected cells were fixed (2% formaldehyde for 15 minutes at room temperature), permeabilized (0.1% Triton X-100 in PBS, pH 7.5, 10 minutes), and blocked (1% BSA in PBS, pH 7.5, 30 minutes) before staining. Cells were then incubated with primary antibodies (mouse anti–human ANGPT1; R&D Systems; MAB9231; 1:100; and mouse anti-FLAG; Sigma-Aldrich; F3165; 1:100) and Alexa Fluor 488–conjugated phalloidin (Invitrogen, Thermo Fisher Scientific) overnight at 4°C before appropriate Alexa Fluor–conjugated secondary antibodies were used to detect FLAG-labeled or native ANGPT1 protein in the cells. DAPI was used for staining of cell nuclei. Images were obtained using a Nikon C2+ confocal microscope. Antibodies against Golgin-97 (CST, D8P2K) and PDI (CST, C81H6) were used to determine the subcellular distribution of the ANGPT1 proteins.

Statistics. Statistical analysis was performed using Prism 5 software (GraphPad). Throughout the text, values are reported as means ± SEM. Indicated *P* values were obtained using a 2-tailed Student's *t* test or ANOVA followed by use of Bonferroni's method for multiple comparisons where appropriate. Comparisons of groups with differing sample sizes were made with Welch's unequal variances *t* test. *P* values of less than 0.05 were considered statistically significant.

Study approval. All animal experiments were approved by the Animal Care Committee at the Center for Comparative Medicine of Northwestern University (Evanston, Illinois, USA). Human subjects and their families were recruited from multiple international centers, which had each received study approval from their respective institutional review boards: University of Wisconsin–Madison Health Sciences Institutional Review Board; Duke University Health System Institutional Review Board for Clinical Investigations, Durham, North Carolina, USA; Children's Hospital of Philadelphia Institutional Review Board, Philadelphia, Pennsylvania, USA; Massachusetts Eye and Ear Infirmary Human Studies Committee; Human Research Ethics Committee of the University of Western Australia; Southern Adelaide Clinical Human Research Ethics Committee, Flinders Medical Centre, Bedford Park, South Australia, Australia; Tasmanian Health and Medical Human Research Ethics Committee, Hobart, Tasmania, Australia; Human Research and Ethics Committee of the Royal Victorian Eye and Ear Hospital; Ethical Review Board of the Medical Faculty of the Friedrich-Alexander University Erlangen-Nürnberg; Ethical Review Board of the Medical Faculty of Niguarda Ca'Granda Hospital, Milan, Italy; and Commission of Ethics for Analysis of Research Projects–Clinical Board of Hospital Clinics and the Faculty of Medicine, University of São Paulo. Written informed consent for study participation was obtained from the subjects or the subjects' parents.

Author contributions

SEQ and TL Young conceived, designed, and supervised the study and wrote the manuscript. BRT designed and performed comparative and developmental biology experiments, analyzed data, and wrote the manuscript. TS designed and performed in vitro experiments, analyzed data, and wrote the manuscript. SWT supervised and performed human genetic analysis, analyzed data, and wrote the manuscript. TO designed and generated the *Angpt1*$^{p.R494^*}$ variant mouse line and contributed to the manuscript. KK, LF, CET, and SJ performed experiments and contributed to the manuscript. OMS, KNW, TL Yanovitch, YSB, LK, DNA, SF, AWH, DAM, JLW, ES, SJ, FP, and JEC contributed human subjects, performed genetic analysis, and contributed to the manuscript. JJ, XL, and SWMJ designed and supervised experiments and contributed to the manuscript. All authors contributed to review and approval of the manuscript.

Acknowledgments

We thank the patient subjects for participating in this study. We also thank John Pater, Joanna Black, Jane Kelly, Sharon Freedman, Ivailo Tournev, and Sylvia Cherninkova for clinical input, Daniel Berner for sequencing assistance, and Veronica Ramirez, Ronnie Anderson, and Andrew Wei for technical assistance. *Angpt1*^{GFP} mice were a gift from Sean Morrison, and *Prox1*^{tdTomato} mice were a gift of Guillermo Oliver. This study was funded by NIH R01 HL124120 and R01 EY025799 (to SEQ); and NIH R01 EY014685, the Research to Prevent Blindness Inc. Lew R. Wasserman Award, and the University of Wisconsin Centennial Scholars Award (to TL Young). This work was also supported by grants from the March of Dimes Foundation and NEI P30EY014104 (to JLW), Howard Hughes Medical Center and EY 11721 (to SJ and KK), the Ophthalmic Research Institute of Australia, the Channel Seven Children's Research Foundation, the Department of Innovation, Industry, Science and Research (Australia), and the National Health and Medical Research Council of Australia. TS is supported by fellowship grants from the Japan Society for the Promotion of Science and Mallinckrodt Pharmaceuticals. Imaging was performed at the Northwestern University Center for Advanced Microscopy supported by NCI CCSG P30 CA060553 awarded to the Robert H. Lurie Comprehensive Cancer Center. This work was supported by the Northwestern University Transgenic and Targeted Mutagenesis Laboratory and a Cancer Center Support Grant (NCI CA060553). We also acknowledge support from Vision Core Grant NEI P30EY016665 and an unrestricted Research to Prevent Blindness grant of the University of Wisconsin–Madison Department of Ophthalmology and Visual Sciences.

Address correspondence to: Susan E. Quaggin, Northwestern University, Feinberg Cardiovascular Research Institute and Division of Nephrology/Hypertension, 303 E. Superior Street, Suite 10-105, Chicago, Illinois 60611, USA. Phone: 312.503.1531; Email: quaggin@northwestern.edu. Or to: Terri L. Young, University of Wisconsin–Madison, Department of Ophthalmology and Visual Sciences, 2828 Marshall Court, Suite 200, Madison, Wisconsin 53705, USA. Phone: 608.263.9797; Email: tyoung6@wisc.edu.

1. Quigley HA, Broman AT. The number of people with glaucoma worldwide in 2010 and 2020. *Br J Ophthalmol*. 2006;90(3):262–267.
2. Coleman AL, Miglior S. Risk factors for glaucoma onset and progression. *Surv Ophthalmol*. 2008;53(suppl 1):S3–S10.
3. Becker B. Tonography in the diagnosis of simple (open angle) glaucoma. *Trans Am Acad Ophthalmol Otolaryngol*. 1961;65:156–162.
4. Park DY, et al. Lymphatic regulator PROX1 determines Schlemm's canal integrity and identity. *J Clin Invest*. 2014;124(9):3960–3974.
5. Kizhatil K, Ryan M, Marchant JK, Henrich S, John SW. Schlemm's canal is a unique vessel with a combination of blood vascular and lymphatic phenotypes that forms by a novel developmental process. *PLoS Biol*. 2014;12(7):e1001912.
6. Aspelund A, et al. The Schlemm's canal is a VEGF-C/VEGFR-3-responsive lymphatic-like vessel. *J Clin Invest*. 2014;124(9):3975–3986.
7. Thomson BR, et al. A lymphatic defect causes ocular hypertension and glaucoma in mice. *J Clin Invest*. 2014;124(10):4320–4324.
8. Souma T, et al. Angiopoietin receptor TEK mutations underlie primary congenital glaucoma with variable expressivity. *J Clin Invest*. 2016;126(7):2575–2587.
9. Augustin HG, Koh GY, Thurston G, Alitalo K. Control of vascular morphogenesis and homeostasis through the angiopoietin-Tie system. *Nat Rev Mol Cell Biol*. 2009;10(3):165–177.
10. Saharinen P, Eklund L, Alitalo K. Therapeutic targeting of the angiopoietin-TIE pathway. *Nat Rev Drug Discov*. 2017;16(9):635–661.
11. Suri C, et al. Requisite role of angiopoietin-1, a ligand for the TIE2 receptor, during embryonic angiogenesis. *Cell*. 1996;87(7):1171–1180.
12. Jeansson M, et al. Angiopoietin-1 is essential in mouse vasculature during development and in response to injury. *J Clin Invest*. 2011;121(6):2278–2289.
13. Barton WA, Dalton AC, Seegar TC, Himanen JP, Nikolov DB. Tie2 and Eph receptor tyrosine kinase activation and signaling. *Cold Spring Harb Perspect Biol*. 2014;6(3):a009142.
14. Gale NW, et al. Angiopoietin-2 is required for postnatal angiogenesis and lymphatic patterning, and only the latter role is rescued by Angiopoietin-1. *Dev Cell*. 2002;3(3):411–423.
15. Dellinger M, et al. Defective remodeling and maturation of the lymphatic vasculature in Angiopoietin-2 deficient mice. *Dev Biol*. 2008;319(2):309–320.
16. Yuan HT, Suri C, Landon DN, Yancopoulos GD, Woolf AS. Angiopoietin-2 is a site-specific factor in differentiation of mouse renal vasculature. *J Am Soc Nephrol*. 2000;11(6):1055–1066.
17. Kurosaki T, Maquat LE. Nonsense-mediated mRNA decay in humans at a glance. *J Cell Sci*. 2016;129(3):461–467.
18. Kim KT, et al. Oligomerization and multimerization are critical for angiopoietin-1 to bind and phosphorylate Tie2. *J Biol Chem*. 2005;280(20):20126–20131.
19. Leppänen VM, Saharinen P, Alitalo K. Structural basis of Tie2 activation and Tie2/Tie1 heterodimerization. *Proc Natl Acad Sci U S A*. 2017;114(17):4376–4381.
20. Moore JO, Lemmon MA, Ferguson KM. Dimerization of Tie2 mediated by its membrane-proximal FNIII domains. *Proc Natl Acad Sci U S A*. 2017;114(17):4382–4387.
21. Procopio WN, Pelavin PI, Lee WM, Yeilding NM. Angiopoietin-1 and -2 coiled coil domains mediate distinct homo-oligomerization patterns, but fibrinogen-like domains mediate ligand activity. *J Biol Chem*. 1999;274(42):30196–30201.
22. Seegar TC, et al. Tie1-Tie2 interactions mediate functional differences between angiopoietin ligands. *Mol Cell*. 2010;37(5):643–655.
23. Felcht M, et al. Angiopoietin-2 differentially regulates angiogenesis through TIE2 and integrin signaling. *J Clin Invest*. 2012;122(6):1991–2005.
24. Hakanpaa L, et al. Endothelial destabilization by angiopoietin-2 via integrin β1 activation. *Nat Commun*. 2015;6:5962.
25. Thurston G, et al. Angiopoietin 1 causes vessel enlargement, without angiogenic sprouting, during a critical developmental period. *Development*. 2005;132(14):3317–3326.
26. Zhu WH, MacIntyre A, Nicosia RF. Regulation of angiogenesis by vascular endothelial growth factor and angiopoietin-1 in the rat aorta model: distinct temporal patterns of intracellular signaling correlate with induction of angiogenic sprouting. *Am J Pathol*. 2002;161(3):823–830.
27. Vikkula M, et al. Vascular dysmorphogenesis caused by an activating mutation in the receptor tyrosine kinase TIE2. *Cell*. 1996;87(7):1181–1190.
28. Limaye N, et al. Somatic mutations in angiopoietin receptor gene TEK cause solitary and multiple sporadic venous malformations. *Nat Genet*. 2009;41(1):118–124.
29. Truong TN, Li H, Hong YK, Chen L. Novel characterization and live imaging of Schlemm's canal expressing Prox-1. *PLoS One*. 2014;9(5):e98245.
30. Ramos RF, Hoying JB, Witte MH, Stamer WD. Schlemm's canal endothelia, lymphatic, or blood vasculature? *J Glaucoma*. 2007;16(4):391–405.
31. Bjarnegård M, et al. Endothelium-specific ablation of PDGFB leads to pericyte loss and glomerular, cardiac and placental abnormalities. *Development*. 2004;131(8):1847–1857.
32. Nguyen LS, Wilkinson MF, Gecz J. Nonsense-mediated mRNA decay: inter-individual variability and human disease. *Neurosci Biobehav Rev*. 2014;46(pt 2):175–186.
33. Belteki G, et al. Conditional and inducible transgene expression in mice through the combinatorial use of Cre-mediated recombination and tetracycline induction. *Nucleic Acids Res*. 2005;33(5):e51.
34. Pyzocha NK, Ran FA, Hsu PD, Zhang F. RNA-guided ing of mammalian cells. In: Storici F, ed. *Gene Correction: Methods and Protocols.* Totowa, New Jersey, USA: Humana Press; 2014:269–277.
35. John SW, Hagaman JR, MacTaggart TE, Peng L, Smithes O. Intraocular pressure in inbred mouse strains. *Invest Ophthalmol Vis Sci*. 1997;38(1):249–253.
36. Feng L, et al. Sustained ocular hypertension induces dendritic degeneration of mouse retinal ganglion cells that depends on cell type and location. *Invest Ophthalmol Vis Sci*. 2013;54(2):1106–1117.
37. Schindelin J, et al. Fiji: an open-source platform for biological-image analysis. *Nat Methods*. 2012;9(7):676–682.
38. Smith RS, Zabaleta A, Savinova OV, John SW. The mouse anterior chamber angle and trabecular meshwork develop without cell death. *BMC Dev Biol*. 2001;1:3.
39. Zhou BO, Ding L, Morrison SJ. Hematopoietic stem and progenitor cells regulate the regeneration of their niche by secreting Angiopoietin-1. *Elife*. 2015;4:e05521.
40. Truman LA, et al. ProxTom lymphatic vessel reporter mice reveal Prox1 expression in the adrenal medulla, megakaryocytes, and platelets. *Am J Pathol*. 2012;180(4):1715–1725.